



Functional Analysis of the Expanded Phosphodiesterase Gene Family in *Toxoplasma gondii* Tachyzoites

William J. Moss,^a Caitlyn E. Patterson,^a Alexander K. Jochmans,^b  Kevin M. Brown^a

^aDepartment of Microbiology and Immunology, University of Oklahoma Health Sciences Center, Oklahoma City, Oklahoma, USA

^bDepartment of Biology, Rogers State University, Claremore, Oklahoma, USA

ABSTRACT *Toxoplasma* motility is both activated and suppressed by 3',5'-cyclic nucleotide signaling. Cyclic GMP (cGMP) signaling through *Toxoplasma gondii* protein kinase G (TgPKG) activates motility, whereas cyclic AMP (cAMP) signaling through TgPKAc1 inhibits motility. Despite their importance, it remains unclear how cGMP and cAMP levels are maintained in *Toxoplasma*. Phosphodiesterases (PDEs) are known to inactivate cyclic nucleotides and are highly expanded in the *Toxoplasma* genome. Here, we analyzed the expression and function of the 18-member TgPDE family in tachyzoites, the virulent life stage of *Toxoplasma*. We detected the expression of 11 of 18 TgPDEs, confirming prior expression studies. A knockdown screen of the TgPDE family revealed four TgPDEs that contribute to lytic *Toxoplasma* growth (TgPDE1, TgPDE2, TgPDE5, and TgPDE9). Depletion of TgPDE1 or TgPDE2 caused severe growth defects, prompting further investigation. While TgPDE1 was important for extracellular motility, TgPDE2 was important for host cell invasion, parasite replication, host cell egress, and extracellular motility. TgPDE1 displayed a plasma membrane/cytoplasmic distribution, whereas TgPDE2 displayed an endoplasmic reticulum/cytoplasmic distribution. Biochemical analysis of TgPDE1 and TgPDE2 purified from *Toxoplasma* lysates revealed that TgPDE1 hydrolyzes both cGMP and cAMP, whereas TgPDE2 was cAMP specific. Interactome studies of TgPDE1 and TgPDE2 indicated that they do not physically interact with each other or other TgPDEs but may be regulated by kinases and proteases. Our studies have identified TgPDE1 and TgPDE2 as central regulators of tachyzoite cyclic nucleotide levels and enable future studies aimed at determining how these enzymes are regulated and cooperate to control *Toxoplasma* motility and growth.

IMPORTANCE Apicomplexan parasites require motility to actively infect host cells and cause disease. Cyclic nucleotide signaling governs apicomplexan motility, but it is unclear how cyclic nucleotide levels are maintained in these parasites. In search of novel regulators of cyclic nucleotides in the model apicomplexan *Toxoplasma*, we identified and characterized two catalytically active phosphodiesterases, TgPDE1 and TgPDE2, that are important for *Toxoplasma's* virulent tachyzoite life cycle. Enzymes that generate, sense, or degrade cyclic nucleotides make attractive targets for therapies aimed at paralyzing and killing apicomplexan parasites.

KEYWORDS *Toxoplasma gondii*, apicomplexan parasites, cyclic nucleotides

Apicomplexan parasites are obligately intracellular protozoan parasites that cause a variety of deadly diseases, including malaria, cryptosporidiosis, and toxoplasmosis. Several species of *Plasmodium* cause human malaria, such as *Plasmodium falciparum* and *P. vivax*, resulting in hundreds of thousands of deaths annually (1). *Cryptosporidium parvum* and *C. hominis* are the main agents of human cryptosporidiosis, a diarrheal disease that kills tens of thousands of children and infants each year (2). *Toxoplasma gondii* (referred to here as *Toxoplasma*) infections are less deadly but are much more

Editor Silvia N. J. Moreno, University of Georgia

Copyright © 2022 Moss et al. This is an open-access article distributed under the terms of the [Creative Commons Attribution 4.0 International license](https://creativecommons.org/licenses/by/4.0/).

Address correspondence to Kevin M. Brown, kevin-brown@ouhsc.edu.

The authors declare no conflict of interest.

Received 20 September 2021

Accepted 3 January 2022

Published 2 February 2022

widespread. *Toxoplasma* infects and persists within 25 to 30% of the global human population and causes toxoplasmosis, which can be fatal for immunosuppressed individuals or developing fetuses (3). Although apicomplexan parasites cause distinct diseases in numerous organ systems, lytic parasite growth is the primary source of pathogenesis caused by apicomplexan parasites (4). Therefore, a better understanding of how these parasites progress through their lytic cycles will reveal molecular targets for novel therapeutic interventions.

The apicomplexan asexual lytic cycle occurs in five general steps: attachment to a host cell, invasion, formation of the parasitophorous vacuole (PV), intracellular replication, and egress (5). Attachment comprises interactions between parasite and host surface proteins/glycoproteins. Upon firm attachment, secretion of specialized secretory organelles called micronemes and rhoptries embed a ring-like invasion complex into the host cell plasma membrane that forms a transient portal for parasite entry (6). The parasite glideosome, a surface adhesin-linked actin-myosin motor, provides the locomotive force for invasion and other motile processes (5). During invasion, the PV is formed from host plasma membrane (stripped of host proteins) and provides an interface between the parasite and host for parasite effector export, immune subversion, and nutrient acquisition (7–9). Once inside the PV, parasites undergo asexual replication generating up to several dozens of newly formed parasites (4). To conclude the lytic cycle, parasites secrete pore-forming microneme proteins and upregulate motility to egress from the PV and host cell (10). The parasite lytic cycle directly results in tissue destruction, increased parasite burden, and subsequent inflammation that is the cornerstone of apicomplexan virulence and pathogenesis. Therefore, understanding how parasites modulate motility for lytic growth is critical to understanding how they cause disease.

Apicomplexans have adapted second messenger signaling systems to regulate microneme secretion and motility (11–15). Purine cyclic nucleotides (cyclic GMP [cGMP] and cAMP) and ionic calcium (Ca^{2+}) signaling pathways are central regulators of apicomplexan motility, but there are species-dependent variations in how they operate. In general, external signals will stimulate parasite guanylate cyclase(s) to produce cGMP from GTP (16–26). Accumulation of cGMP in the parasite cytosol will activate protein kinase G (PKG), the only known cGMP effector in apicomplexans (27). Catalytically active PKG is required for microneme secretion and motility by stimulating Ca^{2+} flux, and through an unknown mechanism that cannot be bypassed by exogenous Ca^{2+} (28–34). PKG is thought to stimulate release of Ca^{2+} stores by upregulating inositol 1,4,5-trisphosphate (IP_3) signaling and by phosphorylating ICM1, a multipass membrane protein essential for PKG-dependent calcium mobilization (35). Cytosolic Ca^{2+} activates Ca^{2+} -binding proteins that regulate microneme secretion (e.g., calcium-dependent protein kinases, vesicle fusion machinery) and motility (e.g., calmodulins) (36–38). The role of cAMP signaling is less conserved in Apicomplexa, where cAMP signaling through protein kinase A catalytic subunit (PKAc) acts in concert with cGMP and Ca^{2+} for *Plasmodium* invasion (13, 39–43), yet PKAc1 inhibits motility following invasion by negatively regulating Ca^{2+} in *Toxoplasma* (44, 45). In either scenario, it is clear that cyclic nucleotide levels must be tightly controlled for timely motility in Apicomplexa.

There is growing evidence for the importance of cyclic nucleotide turnover in apicomplexan parasites. Phosphodiesterases (PDEs) inactivate cyclic nucleotides through hydrolysis (46) and are conserved in Apicomplexa (47). Studies using mammalian PDE inhibitors provided the first experimental evidence for the importance of apicomplexan PDEs. Zaprinast and BIPPO {5-benzyl-3-isopropyl-1H-pyrazolo[4,3-d]pyrimidin-7(6H)-one} upregulate parasite cGMP-dependent motility, while prolonged treatment is lethal (48). Similarly, 3-isobutyl-1-methylxanthine (IBMX) upregulates parasite cAMP and modulates parasite motility, growth and development, but its effects are likely species and life stage dependent (47, 49, 50). At the single-gene level, most of what is known about apicomplexan PDEs comes from *Plasmodium* research. *Plasmodium*

encodes four PDEs (PDE α , - β , - γ , and - δ) that all degrade cGMP, with PDE β (essential in asexual blood stages) also possessing cAMP hydrolytic activity (13, 51). *Cryptosporidium* also encodes a limited set of PDEs (three), but these have yet to be characterized. In contrast, *Toxoplasma* encodes 18 PDEs of unknown functional significance. Recent expression studies indicated that the *Toxoplasma* PDE family consists of life stage-dependent PDEs with diverse subcellular localizations (44, 52, 53). Similar to *Plasmodium* PDE β (42), *Toxoplasma* PDE8 and PDE9 are dual-specific PDEs, although PDE9 was deemed dispensable for tachyzoite growth (53). It is currently unclear which PDEs are primarily responsible for cGMP and/or cAMP turnover in *Toxoplasma* or whether they are functionally redundant.

To facilitate the functional analysis of the *Toxoplasma* PDE family, we created conditional knockdown lines for each *Toxoplasma gondii* PDE (TgPDE) using a mini-auxin-inducible degron (mAID) system (33). Using this system, we assessed the expression and localization of each TgPDE in the virulent tachyzoite life stage and measured their contributions to lytic growth following conditional knockdown. We determined that TgPDE1 and TgPDE2 were critical for lytic parasite growth and possessed distinct cyclic nucleotide preferences and subcellular distributions. Furthermore, interactome studies of TgPDE1 and TgPDE2 indicated that they may function in unique signaling complexes and receive novel modes of regulation. Taken together, our studies identify TgPDE1 and TgPDE2 as central regulators of tachyzoite cyclic nucleotide levels and enable future studies aimed at determining how these enzymes are regulated and cooperate to control motility for lytic growth.

RESULTS

***Toxoplasma* encodes 18 putative PDEs with diverse domain architectures.**

There are 18 phosphodiesterases encoded in the *Toxoplasma* genome, but their roles in cyclic nucleotide turnover and parasite fitness are largely undetermined. One or more TgPDEs are suspected to be vital to the tachyzoite lytic life cycle, as treatment with human PDE inhibitors, like zaprinast, blocks plaque formation (48) (Fig. S1). Conversely, we noted that the nonselective broad-spectrum human PDE inhibitor IBMX does not inhibit tachyzoite growth at a high concentration (0.5 mM), indicating that inhibition of host PDEs does not significantly impact parasite growth and that zaprinast likely targets an essential TgPDE or subset of TgPDEs (Fig. S1). Furthermore, a genome-wide CRISPR knockout screen indicated that five TgPDEs are potentially important for tachyzoite fitness *in vitro* (phenotype scores < -1) (54). Similarly, TgPDE1 and TgPDE2 are refractory to deletion in tachyzoites, providing strong indirect evidence for their importance (44). Collectively, these findings compelled us to investigate the function of the TgPDE family in *Toxoplasma*.

Adhering to the TgPDE nomenclature designated by Vo et al. (53), we analyzed each TgPDE protein sequence for conserved domains using the NCBI Conserved Domain database (55). We determined that TgPDE proteins ranged from 311 amino acids (aa) (TgPDE14) to 3,476 aa (TgPDE18) in length with variable domain architectures. Each TgPDE contained a single C-terminal PDEase_I domain (pfam00233), which hydrolyze 3',5'-cyclic nucleotides such as cAMP and cGMP (Fig. 1). TgPDE4 and TgPDE16 contained portions of an ion transport domain (pfam00520), suggesting that they may also regulate, or be regulated by, ion transport (Fig. 1). TgPDE2 contained a GAF domain (pfam01590) known to bind cyclic nucleotides and modulate PDE activity (56) (Fig. 1). Low-confidence nonspecific domain fragments (data not shown) were also detected for TgPDE7 (transcriptional regulator ICP4, cl33723), TgPDE9 (transcriptional termination factor Rho, cl36163), TgPDE15 (OCRE, cl23757), and TgPDE18 (MAEBL, cl31754; transcriptional termination factor Rho, cl36163; U2 snRNP auxiliary factor, cl36941). Transmembrane domains within TgPDE proteins were predicted using TOPCONS (57). Except for TgPDE2, TgPDE3, and TgPDE14, all TgPDEs had 2 to 7 transmembrane domains (Fig. 1), suggesting that most TgPDEs are integral membrane proteins. Therefore, the expanded TgPDE family appears well suited to degrade cyclic

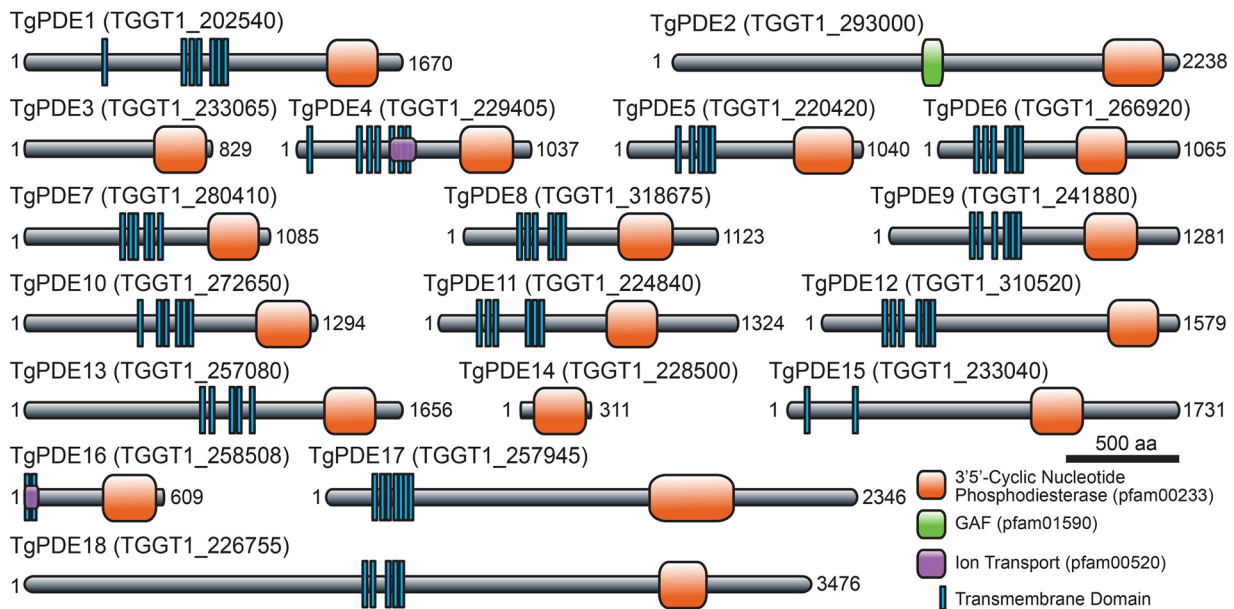


FIG 1 Predicted protein domain architecture of the TgPDE family. Transmembrane domains and conserved protein domains of the 18 putative 3',5'-cyclic nucleotide phosphodiesterases in *T. gondii* based on TOPCONS and NCBI Conserved Domain Database searches.

nucleotides in a variety of subcellular compartments with diverse modes of regulation and secondary functions.

Expression and distribution of TgPDEs in tachyzoites. To investigate the expression of each TgPDE in tachyzoites, we implemented an auxin-inducible degron system for detection and conditional depletion of mAID-3HA (hemagglutinin)-tagged proteins (33). Starting with RH TIR1-3FLAG, which expresses the plant auxin receptor TIR1, we used CRISPR/Cas9 genome editing (58) to tag each *TgPDE* gene with a short homology-flanked *mAID-3HA*, *HXGPRT* cassette (Fig. 2A) as described elsewhere (59). Following drug selection and isolation of clones, genomic DNA was harvested for diagnostic PCRs to distinguish untagged clones from mAID-3HA-tagged clones. Our primer design allowed integration validation such that PCR1 should show only a 283- to 335-bp band in untagged wild-type genomic DNA, while PCR2 should show only a 493- to 534-bp band in TgPDE-mAID-3HA genomic DNA depending on each *TgPDE* gene. Diagnostic PCR revealed that each *TgPDE* was successfully tagged with the *mAID-3HA*, *HXGPRT* for detection and functional analyses (Fig. 2B).

To determine which TgPDEs are expressed in tachyzoites, we used immunofluorescence (IF) microscopy and immunoblotting to detect the 3HA epitope for each TgPDE-mAID-3HA fusion. TgPDE1, -2, -5, -6, -7, -9, -10, -11, -12, -13, and -18 showed expression in tachyzoites by IF microscopy and/or immunoblotting (Fig. 3). We were unable to detect TgPDE8 by either method, but it can be detected with the more sensitive spaghetti monster HA (smHA) tag in tachyzoites (53). Among the TgPDEs detected by IF microscopy, we observed diverse subcellular distribution patterns reminiscent of plasma membrane (TgPDE1, -7, -9, and -10), endoplasmic reticulum (TgPDE2, -11, -13, and -18), mitochondrion (TgPDE5), nucleus (TgPDE6), apical cap (TgPDE9), and cytomembranes (TgPDE1, -2, -6, -10, -11, -13, and -18) (Fig. 3A). Costaining with markers for each compartment and superresolution microscopy will be needed to precisely localize each TgPDE going forward. Of the TgPDEs detected by immunoblotting, all could be detected in full length, but with smaller isoforms also detected for TgPDE2, -7, and -10, indicating that they could be regulated through alternative splicing or proteolysis (Fig. 3B). To determine whether auxin treatment could deplete the TgPDE-mAID-3HA fusions, parasites were treated with vehicle or 0.5 mM auxin (3-indoleacetic acid [IAA]) for 18 h, lysed, and analyzed by SDS-PAGE with immunoblotting for the 3HA epitope.

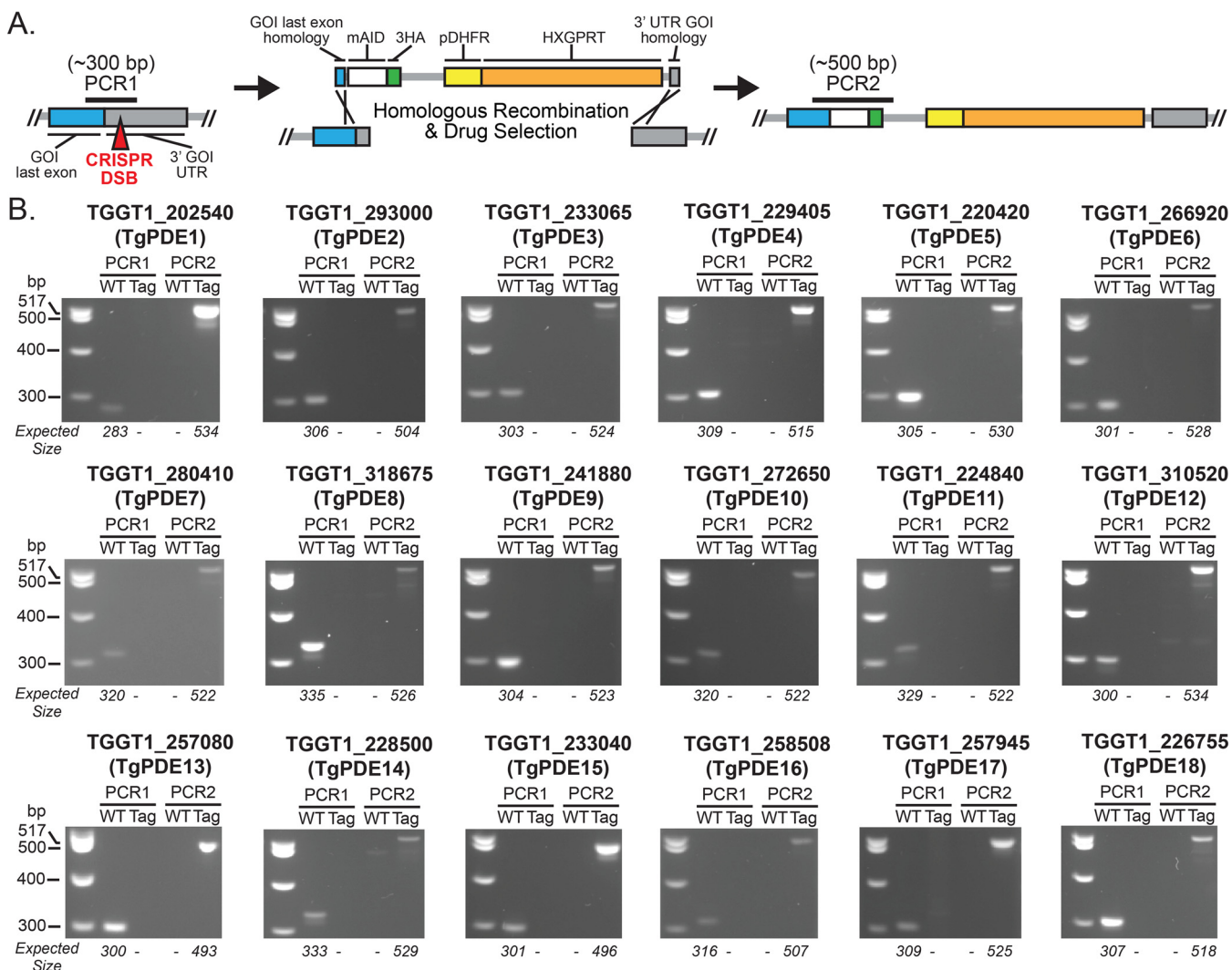


FIG 2 Creation of conditional knockdown lines for all 18 TgPDEs. (A) CRISPR-Cas9 genome editing strategy used to append an *mAID-3HA*, *HXGPRT* cassette (with 40-bp homology flanks) to the 3' end of each *TgPDE* gene in the RH TIR1-3FLAG background. (B) Diagnostic PCR confirmation of successful *mAID-3HA*, *HXGPRT* integration for each *TgPDE* gene. Differential genomic positions of PCR1 and PCR2 are shown in panel A. WT, wild-type parental line RH TIR1-3FLAG. Tag, specific RH TgPDE-*mAID-3HA* clone.

We observed that all detectable TgPDE-*mAID-3HA* fusions were efficiently depleted following auxin treatment (Fig. 3B). Taking all our results together, we have identified at least 11 TgPDEs that may regulate cyclic nucleotide turnover in tachyzoites and have developed a robust knockdown system for assessing the function of each member of the TgPDE family.

Four TgPDEs contribute to the tachyzoite lytic life cycle. To assess the individual contribution of each TgPDE to overall tachyzoite fitness, we performed plaque assays for all 18 TgPDE conditional knockdown mutants. We reasoned that even TgPDEs expressed below the limit of detection may still have important functions, so they were also included in the screen. Freshly harvested RH TIR1-FLAG and RH PDE-*mAID-3HA* tachyzoites were inoculated onto human foreskin fibroblast (HFF) monolayers, treated with 0.5 mM IAA (to deplete *mAID-3HA* fusions) or vehicle for 8 days, fixed with ethanol, and stained with crystal violet to visualize plaque formation (e.g., macroscopic zones of clearance on host cell monolayers). Since plaque formation requires the completion of several rounds of lytic growth, defects in any step of the lytic cycle will reduce plaque formation. As previously reported (33, 38), IAA did not affect the ability of RH TIR1-3FLAG to form plaques (Fig. 4). However, we observed that knockdown of four TgPDEs caused significant plaquing defects compared to vehicle

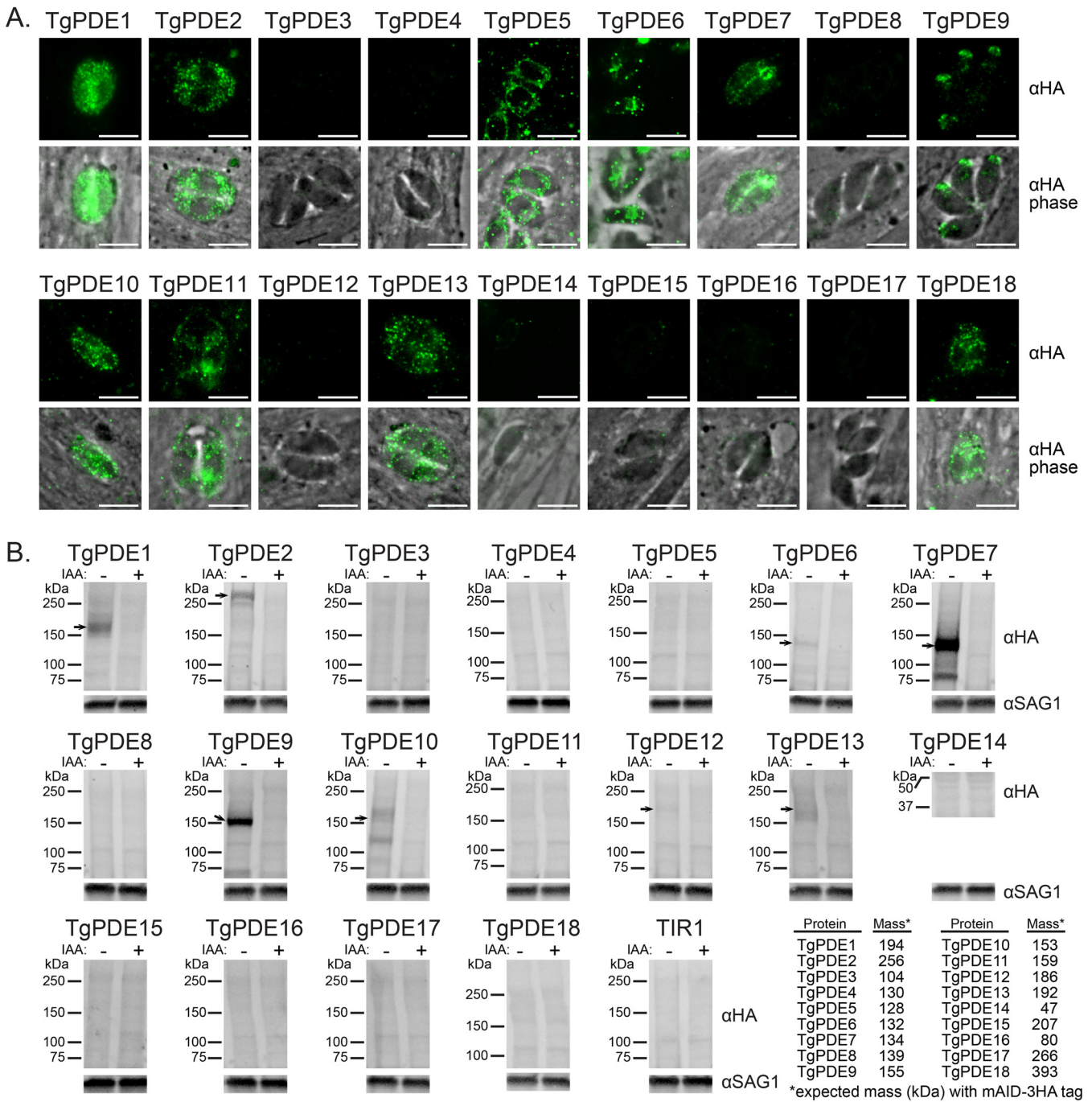


FIG 3 Expression and depletion of TgPDE-mAID-3HA fusions in tachyzoites. (A) IF microscopy of intracellular RH TgPDE-mAID-3HA parasites labeled with mouse anti-HA and goat anti-mouse IgG Alexa Fluor 488. Bar, 5 μ m. (B) Immunoblots of lysates from RH TIR1-3FLAG (TIR1) and RH TgPDE-mAID-3HA (TgPDE) parasites treated with vehicle (EtOH) or 0.5 mM IAA for 18 h. Blots were probed with mouse anti-HA, rabbit anti-SAG1, goat anti-mouse-AFP800, and goat anti-rabbit-AFP680. The table presents the predicted total mass of each TgPDE, including the mAID-3HA tag (12 kDa). Arrows indicate immunoblot-detectable TgPDE-mAID-3HA fusions in tachyzoites.

treatment (Fig. 4). Depletion of TgPDE5 and TgPDE9 reduced plaque area by 32% and 26%, respectively, indicating suboptimal lytic growth (Fig. 4). In contrast, depletion of TgPDE1 and TgPDE2 significantly reduced both plaque area and the number of plaques formed (Fig. 4). TgPDE1 depletion reduced plaque area by 58%, indicating that is critical for tachyzoite growth. TgPDE2 depletion reduced plaque area by 95%, indicating that it may be a master regulator of cAMP and/or cGMP turnover in tachyzoites. The nonredundant phenotypes associated with separate TgPDE1 and TgPDE2

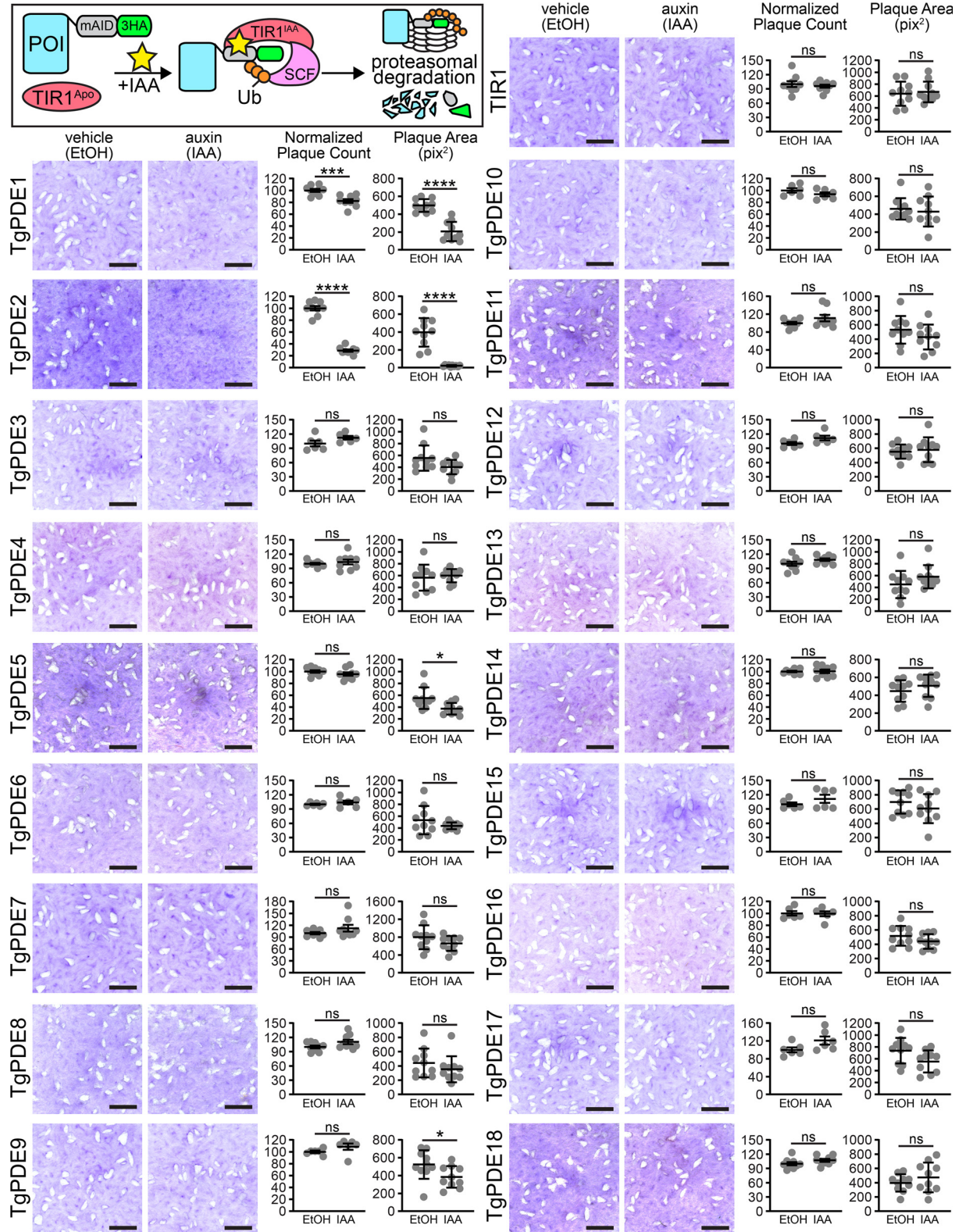


FIG 4 Contribution of each TgPDE to tachyzoite growth. (Inset) Auxin-inducible protein degradation. Plaques formed on HFF monolayers by RH TIR1-3FLAG (TIR1) or derivative RH TgPDE-mAID-3HA lines treated with vehicle (EtOH) or 0.5 mM IAA for 8 days. Bar = 5 mm. Plaque count data are means and standard deviations (SD) ($n = 6$ or 9 replicates, combined from 2 or 3 trials, respectively). For baseline consistency, plaque counts were normalized to 100 vehicle-treated plaques for each line. Plaque area data are means and SD ($n = 10$) from the representative images shown. Unpaired Student's *t* test (ethanol versus IAA) was used. *, $P \leq 0.05$; ***, $P \leq 0.001$; ****, $P \leq 0.0001$; ns, not significant.

depletion suggest that they may have unique cyclic nucleotide preferences which would lead to opposing roles in regulating motility for lytic cycle progression.

Biochemical activities of TgPDEs. To determine the substrate preference of each TgPDE, we first generated recombinant 6His-SUMO fusions of TgPDE catalytic domain fragments (6His-SUMO-TgPDE^{CAT}) from *Escherichia coli*. This strategy was chosen to facilitate expression, solubility, and purification of nondenatured TgPDE^{CAT} fragments based on the retained activity of 6His-PfPDE α ^{CAT}, an analogous fragment of a cGMP-specific PDE from *P. falciparum* purified from *E. coli* (47). For *E. coli* expression, TgPDE^{CAT} fragments (Fig. S2A) were cloned from GT1 tachyzoite cDNA libraries or synthesized as double-stranded DNA (dsDNA) gene fragments and ligated into pET-6His-SUMO (60). Similar constructs containing PfPDE α ^{CAT} and PfPDE β ^{CAT} or HsGSMDM (human gasdermin D) served as positive and negative controls for PDE activity, respectively. The sequence-verified expression constructs were then transformed into SHuffle T7 *E. coli*, induced with isopropylthio- β -galactoside (IPTG), and 6His-SUMO protein fusions were purified from Sarkosyl-solubilized inclusion bodies using immobilized metal affinity chromatography with nickel-nitrilotriacetic acid (Ni-NTA) gravity flow columns (Fig. S2B). The recombinant protein fractions were analyzed by SDS-PAGE with total protein staining, and we determined that each 6His-SUMO-TgPDE^{CAT} protein was captured and adequately purified for downstream analysis (Fig. S3). To determine whether the recombinant 6His-SUMO-TgPDE^{CAT} proteins possessed PDE activity, we performed PDE-Glo assays using cAMP or cGMP as the relevant substrate (Fig. S4A). Unfortunately, we were unable to reliably detect PDE activity for the 6His-SUMO-TgPDE^{CAT} proteins even with 2-h reactions at 37°C (Fig. S4B and C). These results suggest that generating catalytically active recombinant TgPDE^{CAT} proteins will require further optimization (detergents, refolding, etc.) or that TgPDEs need to be purified in full length from *Toxoplasma* to retain activity.

To determine whether endogenously expressed TgPDEs are active, we focused on the two most critical TgPDEs for tachyzoite growth: TgPDE1 and TgPDE2 (Fig. 4). We used immunoprecipitation (IP) to capture TgPDE1-mAID-3HA and TgPDE2-mAID-3HA from native soluble tachyzoite lysates using anti-HA magnetic chromatography with HA peptide elution (Fig. 5A). IP fractions for total protein, soluble protein, and eluted protein were analyzed by immunoblotting, and we observed that TgPDE1 and TgPDE2 were effectively captured (Fig. 5B). We believe the nondenaturing detergents in the native lysis buffer interacted with the transmembrane domains of TgPDE1 and slowed its migration during SDS-PAGE, as has been described for other transmembrane proteins (61, 62). In agreement, the supershifted species of TgPDE1-mAID-3HA was not observed when lysates were prepared without these detergents (Fig. 3B). Due to the nature of the HA peptide elution and relatively low yield of immunoprecipitated proteins, we were unable to measure the exact concentrations of captured proteins. Therefore, we performed PDE-Glo assays using equivalent volumes of IP elution fractions with the untagged parental line elution fraction serving as the background threshold for PDE activity. Upon addition of 200 nM cAMP substrate, eluted TgPDE1 and TgPDE2 fractions were clearly capable of hydrolyzing cAMP compared to the negative control and standards (Fig. 5C). When 20 μ M cGMP substrate was supplied, only eluted TgPDE1 was able to hydrolyze cGMP (Fig. 5D).

To determine if any other TgPDEs were unexpectedly pulled down with TgPDE1-mAID-3HA or TgPDE2-mAID-3HA, we performed similar IP experiments without HA peptide elution and analyzed all captured proteins by liquid chromatography-tandem mass spectrometry (LC-MS/MS) (Fig. S5A). In this case, RH YFP-AID-3HA served as a control for nonspecific protein interactions. IP fractions were first analyzed by total protein staining and immunoblotting (Fig. S5B and C). While the relative abundance of captured protein was low (Fig. S5B), we were able to clearly detect the target proteins by immunoblotting (Fig. S5C). TgPDE1-mAID-3HA and TgPDE2-mAID-3HA both retained hydrolytic activity while immobilized on anti-HA magnetic beads, indicating that native protein complexes were captured (Fig. S5D). Importantly, no other TgPDE coimmunoprecipitated with either TgPDE1 or TgPDE2 in two independent trials (Fig. S5E; Table S4). Furthermore,

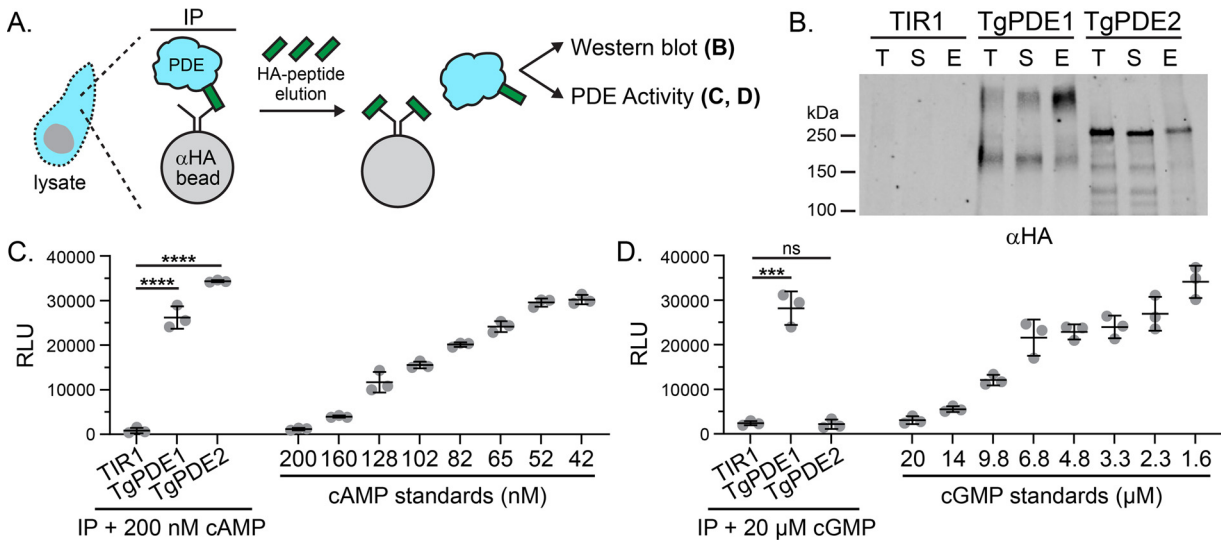


FIG 5 Phosphodiesterase activity of immunoprecipitated TgPDE1 and TgPDE2. (A) Immunoprecipitation strategy for purifying tagged TgPDE1 and TgPDE2 proteins from tachyzoite native lysates. Untagged parental line RH TIR1-3FLAG (TIR1) served as a negative control. (B) Representative immunoblot of immunoprecipitation fractions probed with rat anti-HA and goat anti-rat IRDye 800CW. T, total lysate; S, soluble lysate; E, eluate. (C) Cyclic AMP phosphodiesterase activity of immunoprecipitated elution fractions incubated 1:1 with 0.2 μ M cAMP for 2 h at 37°C. Standards shown were incubated 1:1 with PDE storage buffer for 2 h at 37°C. (D) Cyclic GMP phosphodiesterase activity of immunoprecipitated elution fractions incubated 1:1 with 20 μ M cGMP for 2 h at 37°C. Standards shown were incubated 1:1 with PDE storage buffer for 2 h at 37°C. (C and D) Mean and SD ($n = 3$) from one of four trials ($n = 4$) with similar outcomes. Statistical significance was determined using an unpaired Student's *t* test (TIR1 versus TgPDE1; TIR1 versus TgPDE2). ***, $P \leq 0.001$; ****, $P \leq 0.0001$; ns, not significant.

formaldehyde-cross-linking protein interactions prior to parasite lysis and IP (XL-LC-MS/MS) did not stabilize interactions between TgPDE1 and TgPDE2 or any other TgPDE (Table S5). However, these interactome studies indicate that TgPDE1 and TgPDE2 are potentially regulated by other proteins through protein-protein interactions and/or post-translational modifications.

TgPDE1 and TgPDE2 regulate distinct steps in the lytic cycle. Given that TgPDE1 and TgPDE2 appear nonredundant for tachyzoite growth and have distinct substrates, we speculated that they control distinct steps within the lytic cycle. To test this hypothesis, we performed standard assays for tachyzoite replication, host cell attachment and invasion, host cell egress, and extracellular motility.

To determine whether TgPDE1 and TgPDE2 are important for parasite replication, freshly harvested RH TIR1-3FLAG, RH TgPDE1-mAID-3HA, and RH TgPDE2-mAID-3HA parasites were inoculated onto HFF monolayers for 2 h and then treated with vehicle (ethanol [EtOH]) or 0.5 mM IAA. At 24 h postinfection, the cultures were fixed and immunolabeled with antibodies to TgSAG1, TgGRA7, and the DNA dye Hoechst 33258. Using IF microscopy, we observed that depletion of TgPDE2, but not TgPDE1, reduced the size of the parasite vacuoles and increased the number of irregular vacuoles (Fig. 6A), which contain an atypical number of parasites (non-2N) or parasites with abnormal morphology. To quantify the replication defects, we determined the numbers of regular and irregular vacuoles and the numbers of parasites within each. Depletion of TgPDE1 did not alter the frequency of irregular vacuoles (Fig. 6B) or the number of parasites within each vacuole (Fig. 6B and C). However, depletion of TgPDE2 significantly increased the frequency of irregular vacuoles (Fig. 6B) and decreased the number of parasites in each vacuole (Fig. 6B and C). Since TgPDE2 is capable of degrading cAMP, loss of TgPDE2 could possibly elevate cAMP, resulting in hyperactivation of TgPKAc1. Overexpression of this protein kinase has previously been shown to cause replication defects when overexpressed (44). Since TgPDE1 was dispensable for replication, similar to loss of TgGC (21) and TgPKG (33), it may preferentially regulate cGMP for motility in tachyzoites even though it is capable of degrading both cGMP and cAMP *in vitro*.

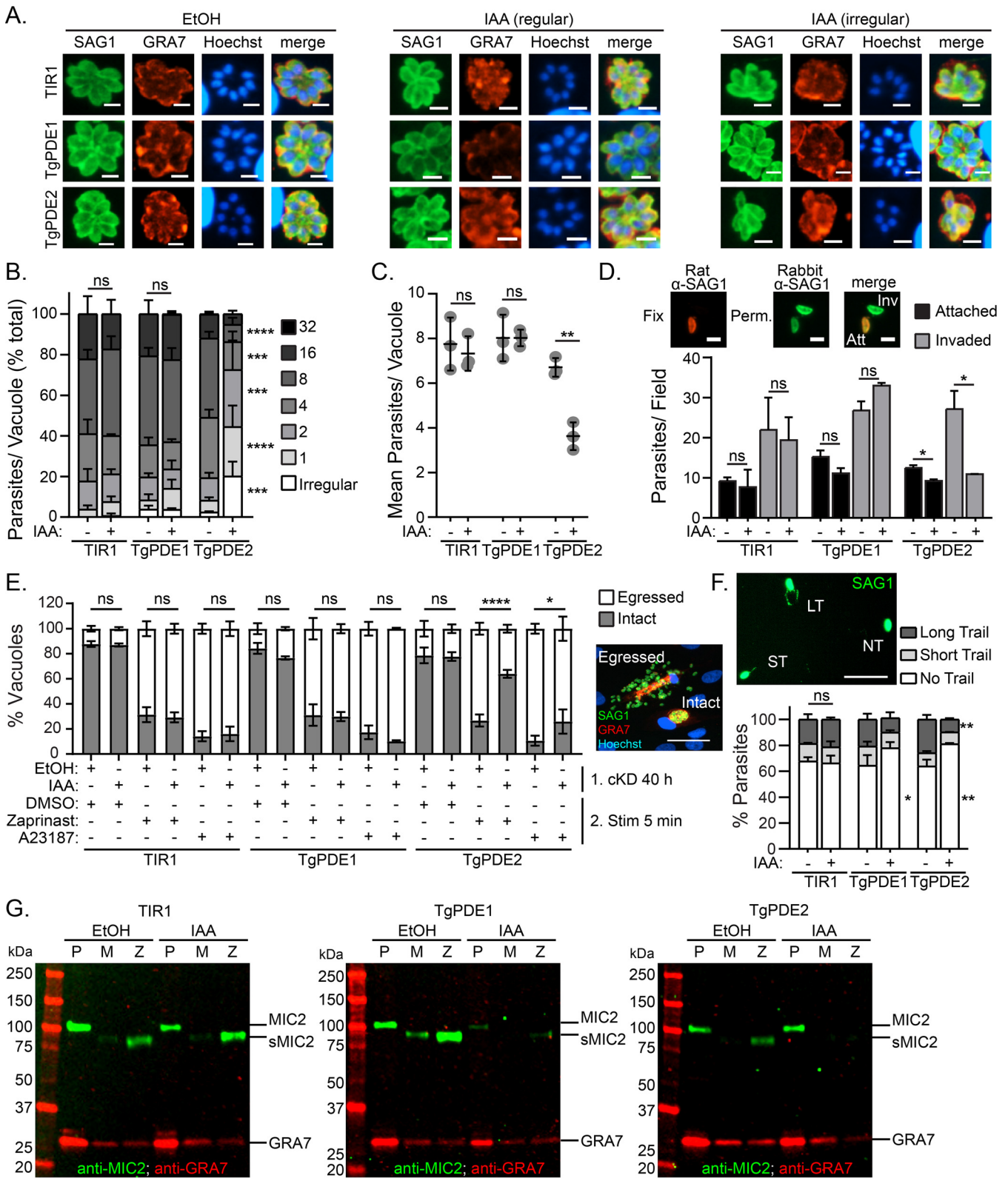


FIG 6 Role of TgPDE1 and TgPDE2 in the tachyzoite lytic cycle. RH TIR1-3FLAG (TIR1) and derivative RH PDE-mAID-3HA parasites (TgPDE1; TgPDE2) were analyzed for defects in the lytic cycle following conditional knockdown of TgPDE1 or TgPDE2 with auxin. (A to C) Replication assay of parasites grown in HFFs treated with vehicle (EtOH) or 0.5 mM IAA for 22 h from 3 independent trials. (A) IF microscopy of fixed parasites labeled with antibodies to TgSAG1, TgGRA7, and the DNA dye Hoechst 33258. Bar = 5 μm. Irregular vacuoles contain an irregular number of parasites or parasites with abnormal morphology. (B) Distribution of parasites per vacuole, with SD. For each line, percentages of parasites in each bin were compared between EtOH and IAA treatment and statistical significance was determined using a two-way ANOVA with Tukey's multiple-comparison test. ***, $P \leq 0.001$; ****, $P \leq 0.0001$; ns, not significant.

(Continued on next page)

To test whether TgPDE1 and TgPDE2 are important for host cell attachment and invasion, we first treated RH TIR1-3FLAG, RH TgPDE1-mAID-3HA, and RH TgPDE2-mAID-3HA cultures with vehicle (EtOH) or 0.5 mM IAA for 16 h. Following knockdown, the treated parasites were purified and allowed to invade fresh HFF monolayers with or without IAA. After 20 min, nonattached parasites were removed and the cultures were fixed. Extracellular and intracellular parasites were differentially labeled with TgSAG1 antibodies and visualized by IF microscopy (Fig. 6D). Surprisingly, TgPDE1 depletion did not significantly affect attachment or invasion. Instead, we found that depletion of TgPDE2 significantly reduced attachment (26% reduction) and invasion (60% reduction) (Fig. 6D). Elevation of cAMP in extracellular tachyzoites by TgPDE2 depletion could lead to premature activation of TgPKAc1, which is known to rapidly suppress *Toxoplasma* motility following invasion (44, 45).

Like invasion, *Toxoplasma* egress requires cGMP and Ca²⁺ signaling. These signals are naturally activated following parasite replication but can also be stimulated by agonists such as the PDE inhibitor zaprinast (a cGMP agonist that also elevates Ca²⁺) and A23187 (a Ca²⁺ agonist). Conversely, cAMP signaling is thought to antagonize egress because genetic inhibition of TgPKAc1 causes premature egress (44, 45). To determine whether TgPDE1 and TgPDE2 are required for egress, we performed an assay that measures natural and agonist-stimulated egress (21). RH TIR1-3FLAG, RH TgPDE1-mAID-3HA, and RH TgPDE2-mAID-3HA were inoculated onto HFFs for 18 h and then treated with vehicle (EtOH) or 0.5 mM IAA to deplete mAID-3HA-tagged proteins. At 40 h, parasites were stimulated with a short pulse of vehicle (dimethyl sulfoxide [DMSO]), 0.5 mM zaprinast, or 2 μ M A23187. Next, the parasite cultures were fixed and immunolabeled with TgSAG1 and TgGRA7 antibodies to detect parasites and vacuoles by IF microscopy (Fig. 6E). At this time point, between 12 and 21% of parasite vacuoles had egressed naturally. In contrast, treatment with zaprinast and A23187 stimulated parasite egress up to 73% and 86%, respectively. Depletion of TgPDE1 increased the percentage of naturally egressed vacuoles from 16% to 23%, but this change was not statistically significant. Modest increases were also observed for stimulated egress when TgPDE1 was depleted, but the differences were also not statistically significant. TgPDE2 depletion did not affect natural egress at 40 h. However, TgPDE2 depletion significantly antagonized zaprinast- and A23187-stimulated egress. Depletion of TgPDE2 reduced zaprinast-induced egress from 73% to 35%, while A23187-induced egress was only reduced from 89% to 74%. These results suggest that TgPDE2 promotes egress by antagonizing cAMP activation of TgPKAc1. In support, inhibition of cGMP signaling through TgPKG blocks premature egress induced by TgPKAc1 genetic inhibition (44).

Following egress, tachyzoites migrate to new host cells using gliding motility (5). To determine whether TgPDE1 and TgPDE2 regulate motility, we first treated RH TIR1-3FLAG, RH TgPDE1-mAID-3HA, and RH TgPDE2-mAID-3HA cultures with vehicle (EtOH) or 0.5 mM IAA for 14 h. Following knockdown, the treated parasites were purified and resuspended in extracellular (EC) buffer with or without EtOH or 0.5 mM IAA. Parasites were allowed to migrate on bovine serum albumin (BSA)-coated wells for 20 min, fixed, and immunolabeled with TgSAG1 antibodies to detect the parasites and their motility

FIG 6 Legend (Continued)

(C) Mean parasites per vacuole and SD. Unpaired Student's *t* test (EtOH versus IAA) was used. **, $P \leq 0.01$. (D) Parasite invasion of HFFs (20 min) following treatment with EtOH or 0.5 mM IAA for 16 h from two or three independent trials. Shown are the mean numbers of attached and invaded parasites per field, with SD, as determined by IF microscopy using differential permeabilization and immunolabeling with rat and rabbit TgSAG1 antibodies. Bar = 5 μ m. Unpaired Student's *t* test (EtOH versus IAA) was used. *, $P \leq 0.05$. (E) Parasite egress from HFFs (40 h) following treatment with EtOH or 0.5 mM IAA for 22 h and stimulation with vehicle (DMSO), 0.5 mM zaprinast, or 2 μ M A23187 for 5 min from 3 independent trials. Shown are the mean percentages of intact and egressed vacuoles with standard errors of the means (SEM) based on IF microscopy using immunolabeling with antibodies against TgSAG1 and TgGRA7. Bar = 100 μ m. Two-way ANOVA with Tukey's multiple-comparison test was used. *, $P \leq 0.05$; ****, $P \leq 0.0001$. (F) Parasite motility on a BSA-coated cover glass in EC buffer following 14 h treatment with EtOH or 0.5 mM IAA. Following a 20-min incubation, parasites were fixed to the cover glass and immunolabeled with TgSAG1 antibodies to detect the parasites and their motility trails by IF microscopy. Shown are mean percentages of parasites and SD with no trail, a short trail (<1 body length), or a long trail (>1 body length) from one of two independent trials. Bar = 30 μ m. Two-way ANOVA with Tukey's multiple-comparison test was used. *, $P \leq 0.05$; **, $P \leq 0.01$. (G) Microneme secretion assay following 14 h treatment with EtOH or 0.5 mM IAA and stimulation with DMSO or 0.5 mM zaprinast in EC buffer for 10 min as detected by immunoblotting with TgMIC2 and TgGRA7 (constitutively secreted control protein) antibodies. Representative immunoblots are shown. P, 10% of unstimulated parasite pellet lysate; M, mock-stimulated secreted fraction; Z, zaprinast-stimulated secreted fraction.

trails by IF microscopy. With vehicle treatment, 32 to 36% of parasites displayed motility trails, which were categorized as short (<1 body length) or long (>1 body length) (Fig. 6F). Depletion of TgPDE1 decreased the percentage of motile parasites from 36% to 23% (Fig. 6F). Depletion of TgPDE2 decreased the percentage of motile parasites from 36% to 19% and the percentage of parasites with long trails from 26% to 10% (Fig. 6F). With respect to their substrate specificities, these results suggest that TgPDE1 and TgPDE2 cooperate to fine-tune cyclic nucleotide levels for proper motility.

Extracellular migration of *Toxoplasma* requires secretion of adhesins (e.g., TgMIC2) from microneme vesicles, permitting substrate-based motility (5). Microneme secretion is dependent on cGMP and Ca²⁺ signaling, which can be strongly upregulated by zaprinast (cGMP agonist) treatment. To better understand why depletion of TgPDE1 and TgPDE2 reduces *Toxoplasma* motility, we examined microneme secretion following TgPDE1 and TgPDE2 knockdown. RH TIR1-3FLAG, RH TgPDE1-mAID-3HA, and RH TgPDE2-mAID-3HA cultures were treated with vehicle (EtOH) or 0.5 mM IAA for 14 h. Following knockdown, the treated parasites were purified and resuspended in EC buffer with or without EtOH or 0.5 mM IAA and incubated with vehicle (DMSO) or 0.5 mM zaprinast for 10 min to facilitate microneme secretion. Parasite pellets and secreted fractions were collected and analyzed by immunoblotting for TgMIC2 and TgGRA7, a constitutively secreted dense granule protein. In vehicle-treated parasites, zaprinast upregulated TgMIC2 secretion compared to mock stimulation (DMSO) (Fig. 6G). Surprisingly, depletion of TgPDE1 reduced the amount of TgMIC2 available for secretion but not the capacity to secrete this smaller pool of TgMIC2 by zaprinast treatment (Fig. 6G). A reduction of microneme proteins within the parasite may be due to premature secretion if cGMP is elevated by TgPDE1 depletion or a general fitness defect. Depletion of TgPDE2 blocked both basal and zaprinast-induced microneme secretion (Fig. 6G). Thus, the motility defects caused by TgPDE1 and TgPDE2 depletion are likely caused by aberrant secretion of micronemes.

Collectively, our investigation of the TgPDE family revealed that TgPDE1 is a dual-specific PDE and TgPDE2 is a cAMP-specific PDE and that both are critical for tachyzoite lytic growth and motility.

DISCUSSION

Recent studies have demonstrated that purine 3',5'-cyclic nucleotides, cGMP and cAMP, are master regulators of lytic life cycle progression in *Toxoplasma* (12, 15). While prior studies focused on the biosynthesis and effector functions of these signaling molecules, here, we focused on an expanded family of PDEs to identify regulators of cyclic nucleotide turnover in *Toxoplasma* (summarized in Table 1). Comparative genomics revealed that coccidian apicomplexans carry 8 to 19 PDE genes, the most out of the four principal apicomplexan groups (gregarines, cryptosporidia, hematozoa, and coccidia) (<https://www.veupathdb.org/>). *Toxoplasma* serves as a tractable model for investigating coccidian PDEs, since it encodes 18 representative PDEs. *Toxoplasma* PDEs have a core domain architecture consisting of a C-terminal PDEase_I domain and variable N-terminal features, although mutational analysis will be needed to identify domains necessary for TgPDE function. By tagging each TgPDE gene with a regulatable epitope tag, we were able to detect 11 TgPDEs expressed in tachyzoites with a variety of subcellular distributions. Our conditional knockdown screen of the TgPDE family revealed that four TgPDEs (TgPDE1, -2, -5, and -9) independently contribute to tachyzoite growth. From these, TgPDE1 and TgPDE2 emerged as principal regulators of tachyzoite fitness. TgPDE1 and TgPDE2 displayed distinct subcellular localizations, cyclic nucleotide preferences, and interactomes, suggesting opposing roles in cyclic nucleotide regulation in tachyzoites. Accordingly, investigation of specific steps within the lytic cycle revealed unique phenotypes associated with depletion of TgPDE1 or TgPDE2.

Studies of PDE function in many apicomplexans have been hindered by the sheer number of PDEs encoded in their genomes. This is especially true for coccidian apicomplexans like *Toxoplasma* that carry 18 PDE genes (Fig. 1). In contrast, other apicomplexan groups, like hematozoa (i.e., malarial parasites and piroplasms), have only 2 to 4 PDE

TABLE 1 Summary of *Toxoplasma* PDE expression, localization, and function

Gene ID	Gene product	Mass (kDa)	Transcript expression TPM (percentile) ^a	Tachyzoite hyperLOPIT (probability) ^b	Tachyzoite distribution by IFA	Tachyzoite fitness score ^c	Tachyzoite cKD/KO phenotypes	cNMP substrate
TGGT1_202540	TgPDE1	182.5	MZ 27.85 (56.3) TZ 70.84 (73.52) BZ 34.79 (64.93)	Golgi (0.75) PM – integral (0.25)	PM ^{ns} Cytomembranes ^{ns}	-2.43	Plaquing ^d =Replication ^d =Attachment ^d =Invasion ^d =Egress ^d Motility ^d MN expression ^d	cGMP ^e cAMP ^e
TGGT1_293000	TgPDE2	243.9	MZ 59.28 (75.98) TZ 27.69 (49.57) BZ 11.43 (41.04)	Nucleus – Chromatin (0.98)	ER ^{ns} Cytomembranes ^{ns}	-2.53	Plaquing ^d Replication ^d Attachment ^d Invasion ^d Egress ^d Motility ^d MN secretion ^d	cAMP ^e
TGGT1_233065	TgPDE3	92.3	MZ 30.45 (59.1) TZ 0.34 (16.86) BZ 0.83 (17.8)	-	ND ^{ns}	-0.65	=Plaquing ^d	-
TGGT1_229405	TgPDE4	118.0	MZ 73.14 (80.03) TZ 2.21 (25.03) BZ 23.25 (55.58)	-	ND ^{ns}	-0.33	=Plaquing ^d	-
TGGT1_220420	TgPDE5	116.1	MZ 2.06 (18.11) TZ 4.56 (27.93) BZ 12.74 (43)	-	ER ^d Cytomembranes ^d Mitochondrion ^d	1.23	Plaquing ^d	-
TGGT1_266920	TgPDE6	119.9	MZ 3.42 (19.96) TZ 399.87 (95.27) BZ 538.83 (96.7)	PM – peripheral 2 (1)	Cytomembranes ^{ns} Nucleus ^d	1.63	=Plaquing ^d	-
TGGT1_280410	TgPDE7	121.6	MZ 7.21 (25.9) TZ 36.41 (56.66) BZ 20.05 (52.25)	Golgi (0.75) PM – integral (0.25)	PM ^{ns} Cytomembranes ^d	0.6	=Plaquing ^d	-
TGGT1_318675	TgPDE8	126.6	MZ 32.06 (60.73) TZ 3.36 (26.5) BZ 13.48 (44.11)	-	Apical PM ^d Cytomembranes ^d ND ^d	0.19	=Plaquing ^d	cGMP ^e cAMP ^e
TGGT1_241880	TgPDE9	142.5	MZ 13.83 (37.77) TZ 84.01 (77.12) BZ 52.08 (72.88)	Apical 1 (0.51) PM – peripheral 2 (0.34) Golgi (0.14)	Apical PM ^{ns}	0.52	Plaquing ^d =Plaquing ^d	cGMP ^e cAMP ^e
TGGT1_272650	TgPDE10	141.3	MZ 5.56 (23.22) TZ 53.07 (66.75) BZ 15.13 (46.39)	PM – integral (0.5) Golgi (0.5)	PM ^{ns} Cytomembranes ^{ns}	-0.37	=Plaquing ^d	-
TGGT1_224840	TgPDE11	146.8	MZ 8.85 (28.99) TZ 30.83 (52.57) BZ 21.76 (53.9)	-	ER ^d Cytomembranes ^d ND ^d	0.4	=Plaquing ^d	-
TGGT1_310520	TgPDE12	174.0	MZ 13.59 (37.29) TZ 7.74 (30.61) BZ 24.58 (56.84)	-	Cytomembranes ^d ND ^d	-0.06	=Plaquing ^d	-
TGGT1_257080	TgPDE13	180.3	MZ 16.77 (42.59) TZ 55.8 (67.98) BZ 22.97 (55.26)	ER (0.56) Golgi (0.42)	ER ^d Basal ^d Cytomembranes ^{ns}	0.55	=Plaquing ^d	-
TGGT1_228500	TgPDE14	35.2	MZ 42.17 (68.08) TZ 0.65 (19.65) BZ 2.64 (23.77)	-	ND ^{ns}	-0.33	=Plaquing ^d	-
TGGT1_233040	TgPDE15	194.9	MZ 39.65 (66.4) TZ 0.79 (20.66) BZ 7.3 (33.65)	-	ND ^{ns}	1.22	=Plaquing ^d	-
TGGT1_258508	TgPDE16	68.4	MZ 146.2 (89.36) TZ 2.37 (25.34) BZ 56.46 (74.36)	-	ND ^{ns}	-1.19	=Plaquing ^d	-
TGGT1_257945	TgPDE17	254.1	MZ 226.54 (92.59) TZ 25.37 (47.43) BZ 24.5 (56.79)	-	ND ^{ns}	-1.81	=Plaquing ^d	-
TGGT1_226755	TgPDE18	381.2	MZ 27.59 (56.03) TZ 6.01 (29.32) BZ 0.46 (15.73)	-	ER ^{ns} Cytomembranes ^{ns}	-1.15	=Plaquing ^d	-

^aRNA-Seq transcript expression from *T. gondii* isolate CZ (type II) in transcripts per million (TPM) with gene-ranked expression percentile for each life-stage: merozoite (MZ, cat EESS [cat endoepithelial stage 5]); tachyzoite (TZ); bradyzoite (BZ) (52).

^bhyperLOPIT subcellular localization from *T. gondii* isolate RH and derivatives using TAGM-MCMC (t- augmented Gaussian mixture models with Markov-chain Monte-Carlo) analysis (65).

^cIFA of TgPDE1 or TgPDE2 C-tagged with 3Ty in intracellular tachyzoites of *T. gondii* line RH $\Delta h x g p r t \Delta k u 8 0$ (44).

^dIFA of TgPDE1-18 C-tagged with spaghetti monster HA (smHA) in intracellular tachyzoites of *T. gondii* line RH $\Delta h x g p r t \Delta k u 8 0$ (53). ND, not detected.

^eIFA of TgPDE1-18 C-tagged with mAID-3HA in intracellular tachyzoites of *T. gondii* line RH TIR1-3FLAG (this study). ND, not detected.

^fMean phenotype score from a genome-wide CRISPR-KO loss of function screen in *T. gondii* line RH Cas9. Negative scores indicate a potential fitness defect associated with gene disruption (54).

^gcKD/KO, conditional knockdown or knockout. Plaques formation, attachment, invasion, egress, motility, microneme (MN) expression, and secretion of *T. gondii* RH TgPDE-mAID-3HA lines treated \pm 0.5 mM IAA (this study). \downarrow , significantly reduced; =, no significant difference.

^hQualitative plaque formation of *T. gondii* RH $\Delta h x g p r t \Delta k u 8 0 \Delta p d e 9$ vs. progenitor (53). =, no difference.

ⁱPDE activity assay (PDE-Glo, Promega) of immunoprecipitated TgPDE1-mAID-3HA and TgPDE2-mAID-3HA (this study).

^jPDE activity assay (colorimetric, Abcam) of immunoprecipitated TgPDE8-smHA and TgPDE9-smHA (53).

genes per species. This discrepancy raises the question of why coccidian apicomplexans need so many PDEs. We speculate that PDE expansion in coccidia meets the demands of their asexual (acute and chronic) and sexual life stages and compartmentalized signaling and serves as a redundancy safeguard for added control. Transcriptome-wide expression studies have indicated a life stage dependence for the majority of TgPDEs (52). In support, 11 of 18 TgPDEs were recently shown to be expressed in tachyzoites by immunofluorescence assay (IFA) and immunoblotting (53), which we were able to largely confirm independently here with disparate epitope tags (Fig. 3). Additional studies are needed to determine which TgPDEs control cyclic nucleotide turnover in other life stages, such as bradyzoites, merozoites, gametes, and sporozoites. We and others have also observed distinct subcellular distributions for TgPDEs (44, 53), indicating that they may act on separate pools of cyclic nucleotides for finely tuned signaling. Previously we showed that cGMP biosynthesis by TgGC and subsequent TgPKG activation occurs at the plasma membrane (21, 33). Therefore, cGMP-TgPDEs positioned at the plasma membrane would be well positioned to turn off TgPKG signaling following invasion. The localization of cAMP signaling is more complex and less centralized in *Toxoplasma* (4 TgACs, 2 TgPKAr, and 3 TgPKAc) (21, 44, 45, 50, 63), which may require compartmentalized TgPDEs to inactivate cAMP signaling for egress or development. Overall, it appears beneficial for *Toxoplasma* to have life stage-dependent PDEs distributed throughout the cell to prevent or inactivate unwanted cyclic nucleotide signaling.

Despite expressing at least 11 TgPDEs in tachyzoites, we were able to identify several TgPDEs that individually contribute to tachyzoite fitness (Fig. 4). It should be noted that we could not confirm knockdown of TgPDEs expressed below the limit of protein detection with our system, which could lead to an underestimation of fitness-conferring TgPDEs. Conditional depletion of TgPDE5 and TgPDE9 modestly reduced the size of plaques formed on HFF monolayers, indicating that they partially contribute to tachyzoite fitness. TgPDE9 was previously determined to be capable of degrading cAMP and cGMP but was deemed dispensable by knockout in tachyzoites (53). Given the time it takes to generate and maintain knockouts, compensatory suppressor mutations could emerge and mask knockout phenotypes. Since TgPDE8 has the same localization and substrate preference as TgPDE9 (53), upregulation of TgPDE8 could feasibly suppress phenotypes associated with $\Delta Tgpd9$. The speed of TgPDE9-mAID-3HA knockdown is unlikely to allow for suppressors, revealing TgPDE9's true contribution to tachyzoite fitness. With loss of TgPDE1, we observed a slight reduction in plaque numbers and the plaques that did form were substantially smaller than those seen with vehicle treatment. The reduction in plaque numbers indicates that TgPDE1 is essential in a subset of parasites within a population of knockdown mutants. TgPDE2 depletion elicited the most severe plaquing defects, reducing plaque size by ~95%. These data indicate that TgPDE1 and TgPDE2 are indispensable and nonredundant for tachyzoite fitness, which supports the hypothesis that TgPDE1 and TgPDE2 are refractory to deletion (44, 54).

To understand how TgPDE1 and TgPDE2 contribute to tachyzoite fitness, we first tested whether either had phosphodiesterase activity. Attempts to generate highly active recombinant TgPDE catalytic domain fragments were unsuccessful (Fig. S2 to S4). We suspect that the recombinant proteins were not adequately refolded following solubilization of inclusion body preparations and will require further optimization. It is also possible that some TgPDEs are simply catalytically inactive or hydrolyze unknown substrates. As an alternative approach, we performed activity assays on tagged TgPDEs immunoprecipitated from *Toxoplasma* lysates (Fig. 5). TgPDE1 was capable of degrading cGMP and cAMP, while TgPDE2 was cAMP specific. It is reasonable for TgPDE1 and TgPDE2 to have different substrate preferences, since they are both required for tachyzoite fitness and likely play nonredundant roles. Our data suggest that TgPDE2 is primarily responsible for cAMP degradation in tachyzoites. Therefore, we speculate that TgPDE1 is primarily responsible for cGMP turnover in tachyzoites, with minor contributions from TgPDE8 and TgPDE9, which are also dual-specific PDEs (53), and possibly

TgPDE5. It is not known whether dual-specific PDEs act selectively in *Toxoplasma*, but they may be important given the mutually exclusive nature of cGMP and cAMP signaling in *Toxoplasma* (12, 15). A combinatorial knockout/knockdown approach is needed to directly address functional redundancy within the TgPDE family.

To ensure that the phosphodiesterase activities we observed for TgPDE1 and TgPDE2 were not artifacts of unexpected interactions with other TgPDEs, we analyzed immunoprecipitated TgPDE1 and TgPDE2 fractions with and without chemical cross-linking by LC-MS/MS (Fig. S5; Table S4 and S5). No other host or *Toxoplasma* PDEs coimmunoprecipitated with TgPDE1 or TgPDE2, indicating that TgPDE1 and TgPDE2 were solely responsible for the cyclic nucleotide degradation observed *ex vivo*. However, we did detect unique interactors for TgPDE1 and TgPDE2 that may regulate their activities through proteolysis, localization, or phosphorylation. Identifying domains and modifications that control TgPDE1 and TgPDE2 activity is critical to understand the mechanisms by which they regulate cyclic nucleotide turnover for lytic growth.

To further dissect and distinguish TgPDE1 and TgPDE2 function, we tested whether they control specific steps or processes within the tachyzoite lytic cycle. We determined that TgPDE1 is important for maintaining proper microneme levels (Fig. 6G) required for extracellular motility (Fig. 6F). Depletion of TgPDE1 may reduce microneme expression through premature microneme secretion or a general fitness defect. Since depletion of TgPDE1 reduced plaque area by 58% without directly diminishing invasion, replication, or egress (Fig. 4), we suspect that these parasites have difficulties spreading to new cells due to decreased motility and/or extracellular survival. Depletion of TgPDE2 was highly pleiotropic, suppressing replication, invasion, egress, motility, and microneme secretion (Fig. 6). The cumulative perturbations of each step in the lytic cycle explains the fewer and 95% smaller plaques observed (Fig. 4). Since TgPDE2 functions as a cAMP-specific PDE (Fig. 5C), we speculate that its depletion elevates cAMP throughout the lytic cycle, causing aberrant activation of TgPKAc1, which is known to antagonize motility and egress normally but can also cause replication defects when overexpressed or hyperactivated (44, 45).

Altogether, our investigation of the 18-member TgPDE family revealed that TgPDE1 and TgPDE2 are the primary phosphodiesterases in *Toxoplasma* tachyzoites. We determined that TgPDE1 is a dual-specific PDE, but we hypothesize that it primarily degrades cGMP in *Toxoplasma*. This work also designates TgPDE2 as the only (to our knowledge) known cAMP-specific PDE in Apicomplexa. We propose a two-part working model in which (i) TgPDE1 is activated following *Toxoplasma* invasion to turn off cGMP-stimulated motility for replication and (ii) TgPDE2 is activated following *Toxoplasma* replication to turn off cAMP signaling, which inhibits motility, for egress and cell-to-cell transmission. This work enables future studies aimed at determining how TgPDE1 and TgPDE2 are regulated and cooperate to control cyclic nucleotide turnover and lytic growth. Furthermore, due to their conservation, TgPDE1 and TgPDE2 will serve as models for coccidian dual-specific and cAMP-specific PDEs, respectively.

MATERIALS AND METHODS

Parasite and host cell culture. *T. gondii* tachyzoites were maintained in human foreskin fibroblast (HFF) monolayers at 37°C and 5% CO₂ in D10 medium (Dulbecco's modified Eagle's medium [Gibco] supplemented with 10% fetal bovine serum [Gibco], 10 mM glutamine [Gibco], and 10 µg/mL gentamicin [Gibco]). Similarly, D3 medium containing 3% fetal bovine serum (FBS) was also used for parasite cultures where indicated. Cell lines were routinely assessed for *Mycoplasma* contamination by PCR using a Myco-Sniff *Mycoplasma* PCR detection kit (MP Biomedicals). All parasite lines used and generated in this study are listed in Table S1.

Antibodies. Mouse anti-HA.11 (clone 16B12) and mouse anti-His tag (clone J099B12) were purchased from BioLegend. Rat anti-HA (clone 3F10) was purchased from Roche. Rabbit anti-TgSAG1 antibodies was provided by John Boothroyd (Stanford University), rat anti-TgSAG1 was provided by Vernon Carruthers (University of Michigan), and rabbit anti-TgGRA7 was provided by David Sibley (Washington University in St. Louis). Goat secondary antibodies conjugated to infrared (IR) dyes and Alexa Fluor dyes were purchased from Li-Cor and Invitrogen, respectively.

Plasmids. All plasmids generated in this study were created by Q5 site-directed mutagenesis (New England Biolabs) of existing plasmids or HiFi Gibson Assembly (New England Biolabs) of linear dsDNA fragments. Plasmid sequences were confirmed by Sanger sequencing (Genewiz) and mapped using SnapGene v5.2.4 (GSL Biotech). All plasmids used in this study are listed in Table S2.

Primers and PCR. All synthetic single-stranded DNA (ssDNA) and dsDNA oligonucleotides were synthesized by Integrated DNA Technologies and are listed in Table S3. Protoscript II reverse transcriptase (New England Biolabs) was used to make cDNA PCR templates from parasite RNA (*Toxoplasma* GT1; *Plasmodium falciparum* NF54) extracted with a Monarch total RNA miniprep kit (New England Biolabs). Genomic DNA (*Toxoplasma* RH derivatives) was extracted for PCR using a Monarch genomic DNA purification kit (New England Biolabs). Q5 polymerase (New England Biolabs) was used for cloning and tagging amplicon PCRs. *Taq* polymerase (New England Biolabs) was used for diagnostic PCRs.

Sequence analysis. Annotated genomic, transcript, and protein sequences for each TgPDE from type I reference strain GT1 were downloaded from <https://www.toxodb.org/>. Transmembrane domains within TgPDE protein sequences were predicted using TOPCONS, a consensus of OCTOPUS, PHILIUS, PolyPhobius, SCAMPI, and SPOCTOPUS algorithms (57). Protein domains and features were predicted using the NCBI conserved domain search against the CDD v3.19 58235 PSSM database with an expect value threshold of 0.01 (55). The predicted transmembrane domains and features were drawn to scale (primary amino acid length) using Adobe Illustrator (Adobe, Inc.).

Generation of TgPDE-mAID-3HA conditional knockdown mutants. RH TIR1-3FLAG tachyzoites were used for tagging TgPDEs with mAID-3HA as described elsewhere (59). To tag each gene of interest (GOI), a *pSAG1:Cas9-GFP, U6:sgGOI 3' UTR* plasmid (2 to 5 μ g) was cotransfected with a corresponding 40-bp homology arm-flanked *mAID-3HA, HXGPRT* amplicon (2 to 5 μ g) into 1×10^6 RH TIR1-3FLAG tachyzoites in P3 buffer using a 4D-nucleofector (Lonza) with pulse code FI-158. Transfected parasites were selected with 25 μ g/mL mycophenolic acid (Alfa Aesar) and 50 μ g/mL xanthine (Alfa Aesar) in D10 medium. Following drug selection, clones were isolated by limiting dilution, and epitope tags were confirmed by diagnostic PCR of genomic DNA.

Knockdown of TgPDE-mAID-3HA protein fusions. Knockdowns were performed as described elsewhere (59). RH TIR1-3FLAG and RH TgPDE-mAID-3HA tachyzoites cultivated in HFFs in D10 medium were treated with 0.5 mM 3-indoleacetic acid (auxin; IAA) (Sigma-Aldrich) prepared in 100% ethanol (Pharmco) or vehicle alone (0.0789% [wt/vol] ethanol final concentration) and incubated at 37°C and 5% CO₂ prior to protein detection and/or phenotypic analysis.

Detection of mAID-3HA-tagged proteins by indirect immunofluorescence microscopy. Tachyzoite-infected HFF monolayers grown on 12-mm number 1 glass coverslips (Electron Microscopy Sciences) were fixed with 4% formaldehyde (Polysciences) in phosphate-buffered saline (PBS), permeabilized with 0.1% Triton X-100 (MP Biomedicals), blocked with 10% normal goat serum (Gibco) in PBS, labeled with mouse anti-HA (1:1,000), and then washed three times with PBS. Antibody-labeled proteins were fluorescently labeled with goat anti-mouse IgG-AF488 (1:2,000), washed five times with PBS, rinsed with water, and mounted on 25- by 75- by 1-mm Superfrost Plus glass slides (VWR) with Prolong Gold (Invitrogen). Wide-field images were captured and analyzed with a 100 \times oil objective on an Axioskop 2 MOT Plus wide-field fluorescence microscope (Carl Zeiss, Inc.) running AxioVision LE64 software (Carl Zeiss, Inc.).

SDS-PAGE and immunoblotting. For routine detection of proteins, tachyzoite pellets were lysed in an equal volume of 2 \times Laemmli buffer (64) containing 20 mM dithiothreitol (DTT) (Thermo Fisher Scientific). All other protein samples were mixed 4:1 with 5 \times Laemmli buffer containing 50 mM DTT. Proteins were separated on 4 to 20% TGX polyacrylamide gels (Bio-Rad) or 4 to 20% TGX Stain-Free polyacrylamide gels (Bio-Rad) by SDS-PAGE. Total protein in polyacrylamide gels was detected using a ChemiDoc MP imaging system (Bio-Rad) using Stain-Free (Bio-Rad) or Oriole (Bio-Rad) stains, as indicated in the figure legends. For immunoblotting, proteins separated by SDS-PAGE in polyacrylamide gels were wet-blotted onto nitrocellulose membranes. The membranes were rinsed with PBS containing 0.1% Tween 20 (PBS-T) and then blocked with PBS-T containing 5% (wt/vol) fat-free powdered milk (blocking buffer). Membranes were probed with primary antibodies diluted in blocking buffer and then washed three times with PBS-T. The membranes were then incubated in the dark with goat IR-dye secondary antibodies (Li-Cor) diluted in blocking buffer with mixing and then washed five times with PBS-T. Membranes were imaged on a ChemiDoc MP imaging system. Gels and membrane blots were analyzed using Image Lab software (Bio-Rad).

Plaque assays. Freshly egressed tachyzoites (RH TIR1-3FLAG and RH PDE-mAID-3HA lines) were harvested, counted on a hemocytometer, and inoculated (200 parasites/well) onto confluent HFF monolayers growing in 6-well plates containing D10 medium. To determine the effect of human phosphodiesterase inhibitors on *Toxoplasma* fitness, wells were treated with 0.5 mM 3-isobutyl-1-methylxanthine (IBMX) (MP Biomedicals) prepared in 100% DMSO (Sigma-Aldrich), 0.5 mM zaprinast (Tocris) prepared in 100% DMSO, or vehicle (0.1% DMSO). To determine the effect of conditional knockdown of a TgPDE on *Toxoplasma* fitness, wells were treated with 0.5 mM IAA or 0.0789% (wt/vol) ethanol (vehicle). In both experiments, plates were left undisturbed for 8 days in a 37°C, 5% CO₂ incubator. Plaque formation was assessed by counting zones of clearance on EtOH-fixed, crystal violet-stained HFF monolayers. Each stained plate was scanned with high-definition digital scanner (Epson) to obtain representative images and for plaque area analysis. For plaque area measurements, the 10 centermost plaques from the representative wells shown were analyzed using ImageJ to define the plaque area in square pixels (pix²).

Replication assays. HFFs were grown to confluence in D10 in 96-well clear-bottom plates (Greiner Bio-One), then inoculated with 2×10^5 tachyzoites in D3 per well, and incubated at 37°C and 5% CO₂. After 2 h, noninvaded parasites were washed away and wells were treated with vehicle (EtOH) or

0.5 mM IAA in D3 at 37°C, 5% CO₂ to degrade the mAID-3HA fusion proteins. At 24 h postinfection, the monolayers were fixed with 4% formaldehyde in PBS for 10 min, permeabilized with cold methanol for 5 min, and blocked with 10% goat serum in PBS. Parasites and vacuoles were labeled with rat anti-TgSAG1 (1:5,000) and rabbit anti-TgGRA7 (1:1,000), respectively. Next, parasites were counterstained with Alexa Fluor-dye conjugated goat secondary antibodies (1:2,000) and Hoechst 33258 dye (1:5000). Sixteen fields were imaged per replicate at 40× using a Cytation 5 plate-reading microscope running Gen5 software (BioTek Instruments). To determine the number of parasites per vacuole, at least 100 vacuoles were counted per replicate and averaged from 3 independent trials.

Invasion assays. Parasites were grown in HFFs in D3 containing vehicle (EtOH) or 0.5 mM IAA for 16 h at 37°C and 5% CO₂ to degrade the mAID-3HA fusion proteins. Treated parasites (4×10^5) were inoculated onto fresh HFF monolayers with or without EtOH or 0.5 mM IAA in 96-well clear-bottom plates, allowed to settle for 10 min, and then incubated at 37°C and 5% CO₂ for 20 min to facilitate invasion. The medium was removed, and the wells were gently washed once with PBS to remove nonattached parasites. Invasion was stopped with 4% formaldehyde in PBS fixation for 10 min, and the monolayer was blocked with 10% normal goat serum in PBS. Extracellular parasites were labeled with rat anti-TgSAG1 (1:5,000); then, the monolayer was permeabilized with cold methanol for 5 min. Intracellular and extracellular parasites were labeled with rabbit anti-TgSAG1 (1:20,000). Following washing, parasites were labeled with Alexa Fluor dye-conjugated secondary antibodies (1:2,000) and Hoechst 33258 dye (1:5,000) and washed again. Sixteen fields were imaged per replicate at ×40 using a Cytation 5 plate-reading microscope running Gen5 software from 2 or 3 trials. Parasites were gated based on red plus green (extracellular) versus green (intracellular) differential staining.

Egress assays. HFFs were grown to confluence in D10 in 96-well clear bottom plates, inoculated with 5×10^3 tachyzoites in fresh D3 per well, and grown in a 37°C, 5% CO₂ incubator. After 18 h, parasites were treated with vehicle (EtOH) or 0.5 mM IAA in D3 to deplete mAID-3HA-tagged proteins. At 40 h, parasites were stimulated with vehicle (DMSO), 0.5 mM zaprinast, or 2 μM A23187 for 5 min in a 37°C, 5% CO₂ incubator. Next, monolayers were prefixed by adding 10% formaldehyde directly to the wells (1:3 dilution) for 5 min. The medium-formaldehyde mixture was removed and fixed with 4% formaldehyde in PBS for 10 min. The fixative was removed, and cold 100% methanol was added to permeabilize the monolayers for 5 min; monolayers were then washed with PBS and blocked with 10% normal goat serum in PBS. Parasites and vacuoles were labeled with rat anti-TgSAG1 (1:5,000) and rabbit anti-TgGRA7 (1:1,000), respectively. Next, parasites were counterstained with Alexa Fluor-dye conjugated goat secondary antibodies (1:2,000) and Hoechst 33258 dye (1:5,000). Twelve fields were imaged per replicate at 20× using a Cytation 5 plate-reading microscope running Gen5 software from 3 independent trials. At least 80 vacuoles were counted per replicate. Vacuoles containing ≥4 parasites were considered intact to exclude reinvaded parasites.

Motility assays. Parasites were grown in HFFs in D3 containing vehicle (EtOH) or 0.5 mM IAA for 14 h at 37°C and 5% CO₂ to degrade the mAID-3HA fusion proteins, then harvested for motility assays on bovine serum albumin (BSA)-coated 96-well clear bottom plates. To coat the wells, 1% (wt/vol) BSA in extracellular (EC) buffer (142 mM NaCl, 1 mM MgCl₂, 1.8 mM CaCl₂, 5.6 mM D-glucose, 25 mM HEPES [pH 7.4]) was added for 2 h at room temperature prior to the start of the assay. Freshly purified treated parasites were counted and resuspended in EC buffer with or without EtOH or 0.5 mM IAA. One hundred microliters of parasite suspension (10^5 parasites) was added to empty BSA-coated wells and allowed to settle for 10 min. Following a 20-min incubation at 37°C and 5% CO₂, parasites were fixed to the wells and immunolabeled with rat anti-TgSAG1 (1:5,000) and goat anti-rat Alexa Fluor 488 (1:2,000) to detect the parasites and their motility trails by IF microscopy. Twenty-five fields were imaged per replicate at ×40 using a Cytation 5 plate-reading microscope running Gen5 software. At least 100 parasites per replicate were examined for TgSAG1-based motility trails and categorized as having no trail, a short trail (<1 body length), or a long trail (>1 body length). Percentages of motile parasites were averaged from two replicates per treatment from 1 of 2 independent trials.

Microneme secretion assays. Parasites were grown in HFFs in D3 containing vehicle (EtOH) or 0.5 mM IAA for 14 h at 37°C and 5% CO₂ to degrade the mAID-3HA fusion proteins and then harvested for microneme secretion assays. Treated parasites were counted and resuspended in EC buffer with or without EtOH or 0.5 mM IAA at 10^8 /mL. A 100-μL aliquot of parasites (10^7 parasites) was lysed with 20 μL 5× Laemmli buffer containing 50 mM DTT to determine the total protein content for subsequent analysis of secreted proteins by immunoblotting. Separately, 100 μL of parasites (10^7 parasites) were incubated with vehicle (DMSO) or 0.5 mM zaprinast for 10 min at 37°C and 5% CO₂ to facilitate microneme secretion, then chilled on ice. Parasites were centrifuged twice at $800 \times g$ and 4°C for 10 min to isolate parasite-free secreted fractions. Fifty microliters of secreted fractions was mixed with 10 μL 5× Laemmli buffer containing 50 mM DTT. Twelve microliters of total protein (diluted 1:10) and 12 μL of secreted fractions were resolved by SDS-PAGE (4 to 20% TGX), transferred to nitrocellulose membranes, and blocked with 5% (wt/vol) milk PBS-T. Membranes were incubated with mouse anti-MIC2 (1:1,000) and rabbit anti-TgGRA7 (1:1,000), washed 3× with PBS-T, and then incubated with IR-dye-conjugated goat secondary antibodies (1:5,000). Following 5 washes in PBS-T, membranes were imaged on a ChemiDoc MP imaging system and analyzed using Image Lab software. Representative images were derived from 1 of 2 independent trials with similar outcomes.

Immunoprecipitation of TgPDE1 and TgPDE2 for activity assays. Freshly egressed tachyzoites (RH TIR1-3FLAG, RH PDE1-mAID-3HA, and RH PDE2-mAID-3HA) from HFF T150 cultures were scraped, syringe lysed three times with a 25-gauge needle to liberate remaining intracellular parasites, and pelleted ($800 \times g$, 4°C, 10 min). Pellets were washed with 30 mL cold PBS, counted on a hemocytometer, and

then pelleted again. Pellets were washed once more with 1 mL cold PBS, transferred to 2 mL tubes, and then pelleted again. Pellets containing $\sim 1 \times 10^8$ parasites were resuspended in 1 mL native lysis buffer (NLB) containing 10 mM K_2HPO_4 , 150 mM NaCl, 5 mM EDTA, 5 mM EGTA (pH 7.4), 0.2% sodium deoxycholate, 1% Triton X-100, and $1 \times$ protease inhibitor cocktail with EDTA (Pierce) and then incubated on ice for 30 min with mixing as described elsewhere (53). Lysates were centrifuged at $14,500 \times g$ and $4^\circ C$ for 20 min to remove insoluble material. The soluble supernatant was added to NLB-washed anti-HA magnetic beads (Pierce; 25 μL slurry per IP) and mixed at $4^\circ C$ for 2 h. A Dynamag (Invitrogen) stand was used to separate beads from supernatant following IP, washing, and elution steps. The beads were washed once with 1 mL NLB, twice with 1 mL PDE storage buffer (40 mM Tris-HCl, 150 mM NaCl [pH 7.5]) containing 0.05% Tween 20, and once with 0.2 mL PDE storage buffer. Immunoprecipitated proteins were eluted from beads with 0.2 mL PDE storage buffer containing 1 mg/mL HA-peptide (Thermo Fisher Scientific) with mixing at $37^\circ C$ for 30 min. Bead-free elution fractions and other IP fractions were stored at $-80^\circ C$ until use.

Immunoprecipitation of TgPDE1 and TgPDE2 for LC-MS/MS protein identification. Freshly egressed tachyzoites (RH YFP-AID-3HA, RH PDE1-mAID-3HA, and RH PDE2-mAID-3HA) from HFF T150 cultures were scraped, syringe lysed three times with a 25-gauge needle to liberate remaining intracellular parasites, and pelleted ($800 \times g$, $4^\circ C$, 10 min). Pellets were washed with 30 mL cold PBS, counted on a hemocytometer, and then pelleted again. For cross-linked IP, parasite pellets were resuspended in cold 6 mL PBS containing 1% formaldehyde and incubated for 10 min. Following cross-linking, parasites were pelleted, resuspended in 6 mL PBS containing 125 mM glycine for 5 min to quench residual formaldehyde, and then pelleted again. Fixed parasite pellets were then resuspended in 30 mL cold PBS. The non-cross-linked and cross-linked parasite suspensions were pelleted and resuspended in 6 mL NLB, syringe disrupted three times with a 25-gauge needle, and then spun at $3200 \times g$ and $4^\circ C$ for 50 min to remove insoluble material. The 6-mL soluble lysate fractions were precleared with NLB-washed anti-c-Myc magnetic beads (Pierce; 50 μL slurry per IP) with mixing for 2 h at $4^\circ C$. The anti-c-Myc beads were removed by centrifugation ($500 \times g$, $4^\circ C$, 10 min), and the precleared soluble lysates were incubated with prewashed anti-HA magnetic beads (Pierce; 50 μL slurry per IP) overnight at $4^\circ C$ with mixing. The anti-HA magnetic beads were centrifuged ($500 \times g$, $4^\circ C$, 10 min) and transferred to 1.5-mL tubes for washing using a Dynamag stand. The beads were washed five times with 1 mL NLB and three times with 1 mL PBS. Dry beads and other IP fractions were stored at $-80^\circ C$ until use. Dry beads containing captured proteins were shipped on dry ice to the Proteomics & Metabolomics Facility at the Center for Biotechnology/University of Nebraska—Lincoln for liquid chromatography with tandem mass spectrometry (LC-MS/MS) protein identification. Specific LC-MS/MS analysis parameters are listed in Table S4 (native IP) and S5 (cross-linked IP), respectively.

Expression and purification of 6His-SUMO-TgPDE^{CAT} proteins. SHuffle T7 competent *E. coli* (New England Biolabs) was transformed with pET-6His-SUMO-[protein] plasmids containing *TgPDE1-18^{CAT}*, *PIPDE α ^{CAT}*, *PIPDE β ^{CAT}*, or *HsGSDMD* fusions (listed in Table S2). Transformed *E. coli* starter cultures were grown overnight at $30^\circ C$ in 50 mL Terrific Broth (TB) (Fisher Scientific) containing 50 $\mu g/mL$ kanamycin with shaking. The cultures were split 1:5 in 250 mL TB containing kanamycin and grown at $30^\circ C$ until reaching an optical density at 600 nm (OD_{600}) between 0.6 and 0.8. The cultures were induced with 1 mM isopropylthio- β -galactoside (IPTG) (Life Technologies) and grown for 4 h at $30^\circ C$. The cells were centrifuged ($12,000 \times g$, $4^\circ C$, 20 min) and the cell pellets were stored at $-20^\circ C$ overnight. The frozen pellets were resuspended in 25 mL cold homogenization buffer: PBS (pH 7.4) containing 10 $\mu L/mL$ Halt EDTA-free protease inhibitor cocktail (Thermo Fisher Scientific) and 2 $\mu L/mL$ Benzonase (Sigma-Aldrich). *E. coli* organisms were homogenized using an Emusiflex-C5 (Avestin) with 6 cycles at 20,000 lb/in². The resulting homogenates were centrifuged ($12,000 \times g$, $4^\circ C$, 20 min), and the insoluble inclusion body fraction was collected (fraction determined to contain recombinant proteins) and solubilized in 4 mL PBS containing 10% (wt/vol) Sarkosyl (MP Biomedicals) with rocking overnight at $4^\circ C$. The samples were diluted 1:10 in 40 mL PBS, and insoluble material was removed by centrifugation ($12,000 \times g$, $4^\circ C$, 20 min). The soluble supernatants were added to 2 mL pre-equilibrated Ni-NTA slurry (Fisher Scientific), incubated for ~ 5 h with mixing, and then loaded onto a 10-mL gravity column (Thermo Fisher Scientific) for washing and elution. The resins were washed twice with 40 mL recombinant wash buffer (40 mM Tris-HCl [pH 7.5] and 5 mM imidazole). The recombinant 6His-SUMO protein fusions were eluted with 3 mL recombinant elution buffer (40 mM Tris-HCl [pH 7.5] and 250 mM imidazole) and concentrated to 500 μL using Amicon Ultra 10-kDa spin columns (Millipore Sigma). The concentrated solutions underwent two buffer exchanges with 500 μL 40 mM Tris-HCl in 0.5 mL Amicon Ultra 10-kDa spin columns to reduce the imidazole concentration from 250 mM to ~ 2.5 mM. The partially purified recombinant proteins were analyzed for purity and identity by SDS-PAGE and immunoblotting with mouse anti-His tag, respectively. Protein concentrations were determined using the Rapid Gold bicinchoninic acid (BCA) protein assay kit (Pierce) measured with a Cytation 5 plate imager running Gen5 software. The recombinant proteins were aliquoted and stored at $-80^\circ C$ until use.

Phosphodiesterase activity assays. To assess the substrate specificity of TgPDEs, recombinant TgPDEs or immunoprecipitated TgPDEs were assayed using the PDE-Glo phosphodiesterase assay kit (Promega) according to the manufacturer's instructions with a few modifications. In brief, cyclic nucleotides were diluted in reaction buffer (40 mM Tris-HCl [pH 7.5], 50 mM $MgCl_2$, 0.5 mg/mL BSA). On ice, 10 μL cAMP (2 or 0.2 μM) or cGMP (20 μM) was combined with 10 μL (1 μg) of purified recombinant 6His-SUMO-PDE^{CAT} protein or 10 μL immunoprecipitated eluate in triplicate to a 96-well nonskirted natural PCR plate (Midwest Scientific). Cyclic nucleotide standards were diluted further in reaction buffer; then, 10 μL of standards were combined with 10 μL PDE storage buffer in triplicate in the same plate.

To initiate the phosphodiesterase reaction, the plates were sealed and incubated at 37°C for 2 h in a T100 thermal cycler (Bio-Rad). After incubation, 10 μ L of the phosphodiesterase reaction was added to a 96-well half-area flat-bottom white polystyrene plate (Greiner) containing 5 μ L termination buffer. Five microliters of detection buffer was added to each reaction, covered with Parafilm, and then incubated at room temperature for 20 min. After incubation, 20 μ L Kinase-Glo was added to the reactions, covered with Parafilm and foil, and incubated at room temperature for 10 min. The resulting luminescence was quantified using a Cytation 5 plate imager running Gen5 software.

Statistical analysis. Data were graphed and analyzed for statistical significance using GraphPad Prism v 9 (GraphPad Software) using a two-tailed Student's *t* test for pairwise comparisons of normally distributed data. A two-way analysis of variance (ANOVA) with Tukey's multiple-comparison test was used for comparing data from multiple treatment conditions with multiple outcomes or observations. Differences between means were considered statistically significant when *P* was <0.05.

Data availability. A merged Scaffold file (.sf3) of all LC-MS/MS data and annotated results is available upon request.

SUPPLEMENTAL MATERIAL

Supplemental material is available online only.

FIG S1, TIF file, 1.2 MB.

FIG S2, TIF file, 1.4 MB.

FIG S3, TIF file, 2.5 MB.

FIG S4, TIF file, 0.7 MB.

FIG S5, TIF file, 2.2 MB.

TABLE S1, DOCX file, 0.01 MB.

TABLE S2, DOCX file, 0.02 MB.

TABLE S3, DOCX file, 0.03 MB.

TABLE S4, XLSX file, 0.05 MB.

TABLE S5, XLSX file, 0.04 MB.

ACKNOWLEDGMENTS

We thank Sophie Alvarez and Michael Naldrett at the Proteomics & Metabolomics Facility (RRID:SCR_021314) at the Center for Biotechnology/University of Nebraska—Lincoln for LC-MS/MS analysis. We thank John Boothroyd (Stanford University) and the *Toxoplasma* community for antibodies and other key reagents used in this study. We thank Josh Beck (Iowa State University) for *Plasmodium falciparum* NF54 lysates. Special thanks go to L. David Sibley (Washington University in St. Louis) for professional guidance and support during the developmental stages of this project.

The facility and instrumentation of the Center for Biotechnology/University of Nebraska—Lincoln are supported by the Nebraska Research Initiative. This research was supported in part by National Institutes of Health NIAID grant K22AI144035 to K.M.B.

REFERENCES

1. Feachem RGA, Chen I, Akbari O, Bertozzi-Villa A, Bhatt S, Binka F, Boni MF, Buckee C, Dieleman J, Dondorp A, Eapen A, Sekhri Feachem N, Filler S, Gething P, Gosling R, Haakenstad A, Harvard K, Hatefi A, Jamison D, Jones KE, Karema C, Kamwi RN, Lal A, Larson E, Lees M, Lobo NF, Micah AE, Moonen B, Newby G, Ning X, Pate M, Quinones M, Roh M, Rolfe B, Shanks D, Singh B, Staley K, Tulloch J, Wegbreit J, Woo HJ, Mpanju-Shumbusho W. 2019. Malaria eradication within a generation: ambitious, achievable, and necessary. *Lancet* 394:1056–1112. [https://doi.org/10.1016/S0140-6736\(19\)31139-0](https://doi.org/10.1016/S0140-6736(19)31139-0).
2. Guerin A, Striepen B. 2020. The biology of the intestinal intracellular parasite *Cryptosporidium*. *Cell Host Microbe* 28:509–515. <https://doi.org/10.1016/j.chom.2020.09.007>.
3. Matta SK, Rinkenberger N, Dunay IR, Sibley LD. 2021. *Toxoplasma gondii* infection and its implications within the central nervous system. *Nat Rev Microbiol* 19:467–480. <https://doi.org/10.1038/s41579-021-00518-7>.
4. White MW, Suvorova ES. 2018. Apicomplexa cell cycles: something old, borrowed, lost, and new. *Trends Parasitol* 34:759–771. <https://doi.org/10.1016/j.pt.2018.07.006>.
5. Frenal K, Dubremetz JF, Lebrun M, Soldati-Favre D. 2017. Gliding motility powers invasion and egress in Apicomplexa. *Nat Rev Microbiol* 15: 645–660. <https://doi.org/10.1038/nrmicro.2017.86>.
6. Shen B, Sibley LD. 2012. The moving junction, a key portal to host cell invasion by apicomplexan parasites. *Curr Opin Microbiol* 15:449–455. <https://doi.org/10.1016/j.mib.2012.02.007>.
7. Clough B, Frickel EM. 2017. The *Toxoplasma* parasitophorous vacuole: an evolving host-parasite frontier. *Trends Parasitol* 33:473–488. <https://doi.org/10.1016/j.pt.2017.02.007>.
8. Matz JM, Beck JR, Blackman MJ. 2020. The parasitophorous vacuole of the blood-stage malaria parasite. *Nat Rev Microbiol* 18:379–391. <https://doi.org/10.1038/s41579-019-0321-3>.
9. Garten M, Beck JR. 2021. Structured to conquer: transport across the Plasmodium parasitophorous vacuole. *Curr Opin Microbiol* 63:181–188. <https://doi.org/10.1016/j.mib.2021.07.010>.
10. Guerra AJ, Carruthers VB. 2017. Structural features of Apicomplexan pore-forming proteins and their roles in parasite cell traversal and egress. *Toxins* 9:265. <https://doi.org/10.3390/toxins9090265>.
11. Lourido S, Moreno SN. 2015. The calcium signaling toolkit of the Apicomplexan parasites *Toxoplasma gondii* and *Plasmodium* spp. *Cell Calcium* 57:186–193. <https://doi.org/10.1016/j.ceca.2014.12.010>.
12. Bullen HE, Bisio H, Soldati-Favre D. 2019. The triumvirate of signaling molecules controlling *Toxoplasma* microneme exocytosis: cyclic GMP, calcium,

- and phosphatidic acid. *PLoS Pathog* 15:e1007670. <https://doi.org/10.1371/journal.ppat.1007670>.
13. Perrin AJ, Patel A, Flueck C, Blackman MJ, Baker DA. 2020. cAMP signalling and its role in host cell invasion by malaria parasites. *Curr Opin Microbiol* 58:69–74. <https://doi.org/10.1016/j.mib.2020.09.003>.
 14. Brochet M, Balestra AC, Brusini L. 2021. cGMP homeostasis in malaria parasites—the key to perceiving and integrating environmental changes during transmission to the mosquito. *Mol Microbiol* 115:829–838. <https://doi.org/10.1111/mmi.14633>.
 15. Uboldi AD, Wilde ML, Bader SM, Tonkin CJ. 2021. Environmental sensing and regulation of motility in *Toxoplasma*. *Mol Microbiol* 115:916–929. <https://doi.org/10.1111/mmi.14661>.
 16. Carucci DJ, Witney AA, Muhia DK, Warhurst DC, Schaap P, Meima M, Li JL, Taylor MC, Kelly JM, Baker DA. 2000. Guanylyl cyclase activity associated with putative bifunctional integral membrane proteins in *Plasmodium falciparum*. *J Biol Chem* 275:22147–22156. <https://doi.org/10.1074/jbc.M001021200>.
 17. Muhia DK, Swales CA, Deng W, Kelly JM, Baker DA. 2001. The gametocyte-activating factor xanthurenic acid stimulates an increase in membrane-associated guanylyl cyclase activity in the human malaria parasite *Plasmodium falciparum*. *Mol Microbiol* 42:553–560. <https://doi.org/10.1046/j.1365-2958.2001.02665.x>.
 18. Hirai M, Arai M, Kawai S, Matsuoka H. 2006. PbGCbeta is essential for *Plasmodium ookinete* motility to invade midgut cell and for successful completion of parasite life cycle in mosquitoes. *J Biochem* 140:747–757. <https://doi.org/10.1093/jb/mvj205>.
 19. Moon RW, Taylor CJ, Bex C, Schepers R, Goulding D, Janse CJ, Waters AP, Baker DA, Billker O. 2009. A cyclic GMP signalling module that regulates gliding motility in a malaria parasite. *PLoS Pathog* 5:e1000599. <https://doi.org/10.1371/journal.ppat.1000599>.
 20. Gao H, Yang Z, Wang X, Qian P, Hong R, Chen X, Su XZ, Cui H, Yuan J. 2018. ISP1-anchored polarization of GCbeta/CDC50A complex initiates malaria ookinete gliding motility. *Curr Biol* 28:2763–2776.E6. <https://doi.org/10.1016/j.cub.2018.06.069>.
 21. Brown KM, Sibley LD. 2018. Essential cGMP signaling in *Toxoplasma* is initiated by a hybrid P-type ATPase-guanylate cyclase. *Cell Host Microbe* 24: 804–816.E6. <https://doi.org/10.1016/j.chom.2018.10.015>.
 22. Bisio H, Lunghi M, Brochet M, Soldati-Favre D. 2019. Phosphatidic acid governs natural egress in *Toxoplasma gondii* via a guanylate cyclase receptor platform. *Nat Microbiol* 4:420–428. <https://doi.org/10.1038/s41564-018-0339-8>.
 23. Yang L, Uboldi AD, Seizova S, Wilde ML, Coffey MJ, Katris NJ, Yamaro-Butte Y, Kocan M, Bathgate RAD, Stewart RJ, McConville MJ, Thompson PE, Botte CY, Tonkin CJ. 2019. An apically located hybrid guanylate cyclase-ATPase is critical for the initiation of Ca(2+) signaling and motility in *Toxoplasma gondii*. *J Biol Chem* 294:8959–8972. <https://doi.org/10.1074/jbc.RA118.005491>.
 24. Gunay-Esiyok O, Scheib U, Noll M, Gupta N. 2019. An unusual and vital protein with guanylate cyclase and P4-ATPase domains in a pathogenic protist. *Life Sci Alliance* 2:e201900402. <https://doi.org/10.26508/lsa.201900402>.
 25. Nofal SD, Patel A, Blackman MJ, Flueck C, Baker DA. 2021. *Plasmodium falciparum* guanylyl cyclase-alpha and the activity of its appended P4-ATPase domain are essential for cGMP synthesis and blood-stage egress. *mBio* 12:e02694-20. <https://doi.org/10.1128/mBio.02694-20>.
 26. Jiang Y, Wei J, Cui H, Liu C, Zhi Y, Jiang Z, Li Z, Li S, Yang Z, Wang X, Qian P, Zhang C, Zhong C, Su XZ, Yuan J. 2020. An intracellular membrane protein GEP1 regulates xanthurenic acid induced gametogenesis of malaria parasites. *Nat Commun* 11:1764. <https://doi.org/10.1038/s41467-020-15479-3>.
 27. Rotella D, Siekierka J, Bhanot P. 2020. *Plasmodium falciparum* cGMP-dependent protein kinase—a novel chemotherapeutic target. *Front Microbiol* 11:610408. <https://doi.org/10.3389/fmicb.2020.610408>.
 28. Billker O, Lourido S, Sibley LD. 2009. Calcium-dependent signaling and kinases in apicomplexan parasites. *Cell Host Microbe* 5:612–622. <https://doi.org/10.1016/j.chom.2009.05.017>.
 29. Lourido S, Tang K, Sibley LD. 2012. Distinct signalling pathways control *Toxoplasma* egress and host-cell invasion. *EMBO J* 31:4524–4534. <https://doi.org/10.1038/emboj.2012.299>.
 30. Collins CR, Hackett F, Strath M, Penzo M, Withers-Martinez C, Baker DA, Blackman MJ. 2013. Malaria parasite cGMP-dependent protein kinase regulates blood stage merozoite secretory organelle discharge and egress. *PLoS Pathog* 9:e1003344. <https://doi.org/10.1371/journal.ppat.1003344>.
 31. Brown KM, Lourido S, Sibley LD. 2016. Serum albumin stimulates protein kinase G-dependent microneme secretion in *Toxoplasma gondii*. *J Biol Chem* 291:9554–9565. <https://doi.org/10.1074/jbc.M115.700518>.
 32. Sidik SM, Hortua Triana MA, Paul AS, El Bakkouri M, Hackett CG, Tran F, Westwood NJ, Hui R, Zuercher WJ, Duraisingh MT, Moreno SN, Lourido S. 2016. Using a genetically encoded sensor to identify inhibitors of *Toxoplasma gondii* Ca2+ signaling. *J Biol Chem* 291:9566–9580. <https://doi.org/10.1074/jbc.M115.703546>.
 33. Brown KM, Long S, Sibley LD. 2017. Plasma membrane association by N-acylation governs PKG function in *Toxoplasma gondii*. *mBio* 8:e00375-17. <https://doi.org/10.1128/mBio.00375-17>.
 34. Fang H, Gomes AR, Klages N, Pino P, Maco B, Walker EM, Zenonos ZA, Angrisano F, Baum J, Doerig C, Baker DA, Billker O, Brochet M. 2018. Epistasis studies reveal redundancy among calcium-dependent protein kinases in motility and invasion of malaria parasites. *Nat Commun* 9:4248. <https://doi.org/10.1038/s41467-018-06733-w>.
 35. Balestra AC, Koussis K, Klages N, Howell SA, Flynn HR, Bantscheff M, Pasquarello C, Perrin AJ, Brusini L, Arboit P, Sanz O, Castano LP, Withers-Martinez C, Hainard A, Ghidelli-Disse S, Snijders AP, Baker DA, Blackman MJ, Brochet M. 2021. Ca(2+) signals critical for egress and gametogenesis in malaria parasites depend on a multipass membrane protein that interacts with PKG. *Sci Adv* 7:eabe5396. <https://doi.org/10.1126/sciadv.abe5396>.
 36. Lourido S, Shuman J, Zhang C, Shokat KM, Hui R, Sibley LD. 2010. Calcium-dependent protein kinase 1 is an essential regulator of exocytosis in *Toxoplasma*. *Nature* 465:359–362. <https://doi.org/10.1038/nature09022>.
 37. Farrell A, Thirugnanam S, Lorestani A, Dvorin JD, Eidell KP, Ferguson DJ, Anderson-White BR, Duraisingh MT, Marth GT, Gubbels MJ. 2012. A DOC2 protein identified by mutational profiling is essential for apicomplexan parasite exocytosis. *Science* 335:218–221. <https://doi.org/10.1126/science.1210829>.
 38. Long S, Brown KM, Drewry LL, Anthony B, Phan IQH, Sibley LD. 2017. Calmodulin-like proteins localized to the conoid regulate motility and cell invasion by *Toxoplasma gondii*. *PLoS Pathog* 13:e1006379. <https://doi.org/10.1371/journal.ppat.1006379>.
 39. Ono T, Cabrita-Santos L, Leitao R, Bettiol E, Purcell LA, Diaz-Pulido O, Andrews LB, Tadakuma T, Bhanot P, Mota MM, Rodriguez A. 2008. Adenylyl cyclase alpha and cAMP signaling mediate *Plasmodium* sporozoite apical regulated exocytosis and hepatocyte infection. *PLoS Pathog* 4:e1000008. <https://doi.org/10.1371/journal.ppat.1000008>.
 40. Dawn A, Singh S, More KR, Siddiqui FA, Pachikara N, Ramdani G, Langsley G, Chitnis CE. 2014. The central role of cAMP in regulating *Plasmodium falciparum* merozoite invasion of human erythrocytes. *PLoS Pathog* 10:e1004520. <https://doi.org/10.1371/journal.ppat.1004520>.
 41. Furuyama W, Enomoto M, Mossaad E, Kawai S, Mikoshiba K, Kawazu S. 2014. An interplay between 2 signaling pathways: melatonin-cAMP and IP3-Ca2+ signaling pathways control intraerythrocytic development of the malaria parasite *Plasmodium falciparum*. *Biochem Biophys Res Commun* 446:125–131. <https://doi.org/10.1016/j.bbrc.2014.02.070>.
 42. Flueck C, Drought LG, Jones A, Patel A, Perrin AJ, Walker EM, Nofal SD, Snijders AP, Blackman MJ, Baker DA. 2019. Phosphodiesterase beta is the master regulator of cAMP signalling during malaria parasite invasion. *PLoS Biol* 17:e3000154. <https://doi.org/10.1371/journal.pbio.3000154>.
 43. Patel A, Perrin AJ, Flynn HR, Bisson C, Withers-Martinez C, Treeck M, Flueck C, Nicastro G, Martin SR, Ramos A, Gilberger TW, Snijders AP, Blackman MJ, Baker DA. 2019. Cyclic AMP signalling controls key components of malaria parasite host cell invasion machinery. *PLoS Biol* 17:e3000264. <https://doi.org/10.1371/journal.pbio.3000264>.
 44. Jia Y, Marq JB, Bisio H, Jacot D, Mueller C, Yu L, Choudhary J, Brochet M, Soldati-Favre D. 2017. Crosstalk between PKA and PKG controls pH-dependent host cell egress of *Toxoplasma gondii*. *EMBO J* 36:3250–3267. <https://doi.org/10.15252/emboj.201796794>.
 45. Uboldi AD, Wilde ML, McRae EA, Stewart RJ, Dagley LF, Yang L, Katris NJ, Hapuarachchi SV, Coffey MJ, Lehane AM, Botte CY, Waller RF, Webb AI, McConville MJ, Tonkin CJ. 2018. Protein kinase A negatively regulates Ca2+ signalling in *Toxoplasma gondii*. *PLoS Biol* 16:e2005642. <https://doi.org/10.1371/journal.pbio.2005642>.
 46. Soderling SH, Beavo JA. 2000. Regulation of cAMP and cGMP signaling: new phosphodiesterases and new functions. *Curr Opin Cell Biol* 12: 174–179. [https://doi.org/10.1016/s0955-0674\(99\)00073-3](https://doi.org/10.1016/s0955-0674(99)00073-3).
 47. Yuasa K, Mi-Ichi F, Kobayashi T, Yamanouchi M, Kotera J, Kita K, Omori K. 2005. PfpDE1, a novel cGMP-specific phosphodiesterase from the human malaria parasite *Plasmodium falciparum*. *Biochem J* 392:221–229. <https://doi.org/10.1042/BJ20050425>.

48. Howard BL, Harvey KL, Stewart RJ, Azevedo MF, Crabb BS, Jennings IG, Sanders PR, Manalack DT, Thompson PE, Tonkin CJ, Gilson PR. 2015. Identification of potent phosphodiesterase inhibitors that demonstrate cyclic nucleotide-dependent functions in apicomplexan parasites. *ACS Chem Biol* 10:1145–1154. <https://doi.org/10.1021/cb501004q>.
49. Kebaier C, Vanderberg JP. 2010. Initiation of *Plasmodium* sporozoite motility by albumin is associated with induction of intracellular signalling. *Int J Parasitol* 40:25–33. <https://doi.org/10.1016/j.ijpara.2009.06.011>.
50. Sugi T, Ma YF, Tomita T, Murakoshi F, Eaton MS, Yakubu R, Han B, Tu V, Kato K, Kawazu S, Gupta N, Suvorova ES, White MW, Kim K, Weiss LM. 2016. *Toxoplasma gondii* cyclic AMP-dependent protein kinase subunit 3 is involved in the switch from tachyzoite to bradyzoite development. *mBio* 7:e00755-16. <https://doi.org/10.1128/mBio.00755-16>.
51. Baker DA, Drought LG, Flueck C, Nofal SD, Patel A, Penzo M, Walker EM. 2017. Cyclic nucleotide signalling in malaria parasites. *Open Biol* 7:170213. <https://doi.org/10.1098/rsob.170213>.
52. Hehl AB, Basso WU, Lippuner C, Ramakrishnan C, Okoniewski M, Walker RA, Grigg ME, Smith NC, Deplazes P. 2015. Asexual expansion of *Toxoplasma gondii* merozoites is distinct from tachyzoites and entails expression of non-overlapping gene families to attach, invade, and replicate within feline enterocytes. *BMC Genomics* 16:66. <https://doi.org/10.1186/s12864-015-1225-x>.
53. Vo KC, Gunay-Esiyok O, Liem N, Gupta N. 2020. The protozoan parasite *Toxoplasma gondii* encodes a gamut of phosphodiesterases during its lytic cycle in human cells. *Comput Struct Biotechnol J* 18:3861–3876. <https://doi.org/10.1016/j.csbj.2020.11.024>.
54. Sidik SM, Huet D, Ganesan SM, Huynh MH, Wang T, Nasamu AS, Thiru P, Saeij JJP, Carruthers VB, Niles JC, Lourido S. 2016. A genome-wide CRISPR screen in *Toxoplasma* identifies essential apicomplexan genes. *Cell* 166:1423–1435.E12. <https://doi.org/10.1016/j.cell.2016.08.019>.
55. Lu S, Wang J, Chitsaz F, Derbyshire MK, Geer RC, Gonzales NR, Gwadz M, Hurwitz DI, Marchler GH, Song JS, Thanki N, Yamashita RA, Yang M, Zhang D, Zheng C, Lanczycki CJ, Marchler-Bauer A. 2020. CDD/SPARCLE: the conserved domain database in 2020. *Nucleic Acids Res* 48:D265–D268. <https://doi.org/10.1093/nar/gkz991>.
56. Schultz JE. 2009. Structural and biochemical aspects of tandem GAF domains. *Handb Exp Pharmacol* 6:93–109. https://doi.org/10.1007/978-3-540-68964-5_6.
57. Tsigiris KD, Peters C, Shu N, Kall L, Elofsson A. 2015. The TOPCONS web server for consensus prediction of membrane protein topology and signal peptides. *Nucleic Acids Res* 43:W401–W407. <https://doi.org/10.1093/nar/gkv485>.
58. Shen B, Brown KM, Lee TD, Sibley LD. 2014. Efficient gene disruption in diverse strains of *Toxoplasma gondii* using CRISPR/CAS9. *mBio* 5:e01114-14. <https://doi.org/10.1128/mBio.01114-14>.
59. Brown KM, Long S, Sibley LD. 2018. Conditional knockdown of proteins using auxin-inducible degron (AID) fusions in *Toxoplasma gondii*. *Bio Protoc* 8:e2728. <https://doi.org/10.21769/BioProtoc.2728>.
60. Kambara H, Liu F, Zhang X, Liu P, Bajrami B, Teng Y, Zhao L, Zhou S, Yu H, Zhou W, Silberstein LE, Cheng T, Han M, Xu Y, Luo HR. 2018. Gasdermin D exerts anti-inflammatory effects by promoting neutrophil death. *Cell Rep* 22:2924–2936. <https://doi.org/10.1016/j.celrep.2018.02.067>.
61. Rath A, Glibowicka M, Nadeau VG, Chen G, Deber CM. 2009. Detergent binding explains anomalous SDS-PAGE migration of membrane proteins. *Proc Natl Acad Sci U S A* 106:1760–1765. <https://doi.org/10.1073/pnas.0813167106>.
62. Matsumoto H, Haniu H, Komori N. 2019. Determination of protein molecular weights on SDS-PAGE. *Methods Mol Biol* 1855:101–105. https://doi.org/10.1007/978-1-4939-8793-1_10.
63. Mueller C, Samoo A, Hammoudi PM, Klages N, Kallio JP, Kursula I, Soldati-Favre D. 2016. Structural and functional dissection of *Toxoplasma gondii* armadillo repeats only protein. *J Cell Sci* 129:1031–1045.
64. Laemmli UK. 1970. Cleavage of structural proteins during the assembly of the head of bacteriophage T4. *Nature* 227:680–685. <https://doi.org/10.1038/227680a0>.
65. Barylyuk K, Koreny L, Ke H, Butterworth S, Crook OM, Lassadi I, Gupta V, Tromer E, Mourier T, Stevens TJ, Breckels LM, Pain A, Lilley KS, Waller RF. 2020. A comprehensive subcellular atlas of the *Toxoplasma* proteome via hyperLOPIT provides spatial context for protein functions. *Cell Host Microbe* 28:752–766.E9. <https://doi.org/10.1016/j.chom.2020.09.011>.